Foehn Winds at Pine Island Glacier and their role in Ice Changes

Diana Francis[1*], Ricardo Fonseca[1], Kyle S. Mattingly[2], Stef Lhermitte[3,5], Catherine Walker[4]

[1] The Environmental and Geophysical Sciences (ENGEOS) Lab, Khalifa University, P. O. Box 127788, Abu Dhabi, United Arab Emirates.
[2] Space Science and Engineering Center, University of Wisconsin-Madison, Madison, WI, USA.
[3] Department of Earth & Environmental Sciences, KU Leuven, Belgium.
[4] Department of Applied Ocean Physics and Engineering, Woods Hole Oceanographic Institution, Woods Hole, MA, USA.
[5] Department of Geosciences & Remote Sensing, Delft University of Technology, Netherlands.

*Corresponding author: diana.francis@ku.ac.ae

Abstract

Pine Island Glacier (PIG) has recently experienced increased ice loss mostly attributed to basal melt and ocean-ice dynamics. However, atmospheric forcing also plays a role in the ice mass budget, as besides lower-latitude warm air intrusions, the steeply sloping terrain that surrounds the glacier promotes frequent Foehn winds. An investigation of 41-years of reanalysis data reveals that Foehn occurs more frequently from June to October, with Foehn episodes typically lasting about 5 to 9 h. An analysis of the surface mass balance indicated that their largest impact is on the surface sublimation, which is increased by about 1.4 mm water equivalent (w.e.) day^{-1} with respect to no-Foehn events. Blowing snow makes roughly the same contribution as snowfall, around 0.34-0.36 mm w.e. day^{-1}, but with the opposite sign. The melting rate is three orders of magnitude smaller than the surface sublimation rate. The negative phase of the Antarctic Oscillation and the positive phase of the Southern Annular Mode promote the occurrence of Foehn at PIG. A particularly strong event took place on 09-11 November 2011, when 10-m winds speeds in excess of 20 m s^{-1} led to downward sensible heat fluxes higher than 75 W m^{-2} as they descended the mountainous terrain. Surface sublimation and blowing snow sublimation dominated the surface mass balance, with magnitudes of up to 0.13 mm w.e. hr^{-1}. Satellite data indicated an hourly surface melting area exceeding 100 km^2. Our results stress the importance of the atmospheric forcing on the ice mass balance at PIG.

Keywords: Pine Island Glacier, Foehn Winds, Amundsen Sea Low, Snow Sublimation, Surface Mass Balance, Ice Loss.

1. Introduction

The West Antarctic Ice Sheet and its marine terminating ice shelves have been thinning rapidly in the last few decades, contributing to roughly 10% of the observed global mean sea-level rise (Jenkins et al., 2010; Smith et al., 2020). A collapse of the West Antarctic Ice Sheet alone is estimated to lead to a 3 m rise in the global sea-level (Bamber et al., 2009b), and model simulations suggest it can be initiated by an ocean warming of approximately 1.2ºC (Rosier et al., 2021). One of the main contributors to the ice loss in West Antarctica is Pine Island Glacier (PIG), Fig. 1a, which is presently Antarctica's single largest contributor to sea-level rise (Favier et al., 2014; Joughin et al., 2021; Lhermitte et al., 2021). Over the last two decades PIG has lost more than a trillion tons of ice, which corresponds to a roughly 3 mm rise in sea-level (De Rydt et al., 2021). Satellite images indicate a jump in the average volume loss rate around PIG from roughly 2.6 $km^3 y^{-1}$ in 1995 to 10.1 $km^3 y^{-1}$ in 2006 (Wingham et al., 2009), with recent studies stressing a further speedup of ice loss since 2017 (Joughin et al., 2021; Lhermitte et al., 2021; Nilsson et al., 2022). In fact, Li et al. (2022) reported a decrease in elevation around PIG, as estimated from satellite measurements, at a rate of approximately -2 ± 0.04 $m y^{-1}$ from 2016 to 2019. Satellite data indicates an ice velocity magnitude in excess of 200 $m y^{-1}$ over a broad region, Fig. 1a, with peak values higher than 4.5 $km y^{-1}$ (Liu et al., 2022). The ice loss at PIG can be seen by the rapid retreat of the ice front, Fig. 1b, in particular since 2015, with major calving events taking place in October-November 2018 and February 2020 (Liu et al., 2022; Lhermitte et al., 2021).

(a)

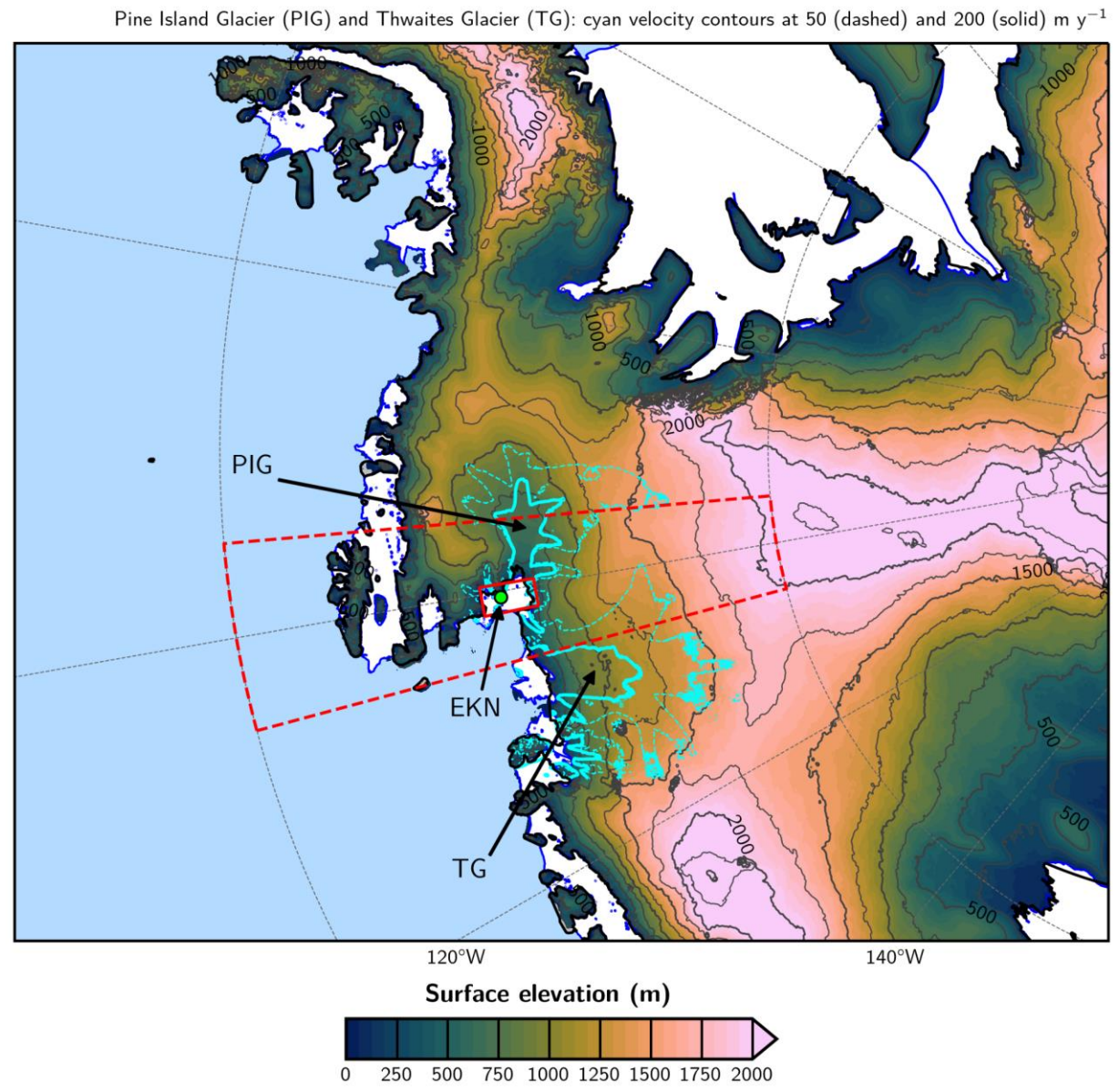
Pine Island Glacier (PIG) and Thwaites Glacier (TG): cyan velocity contours at 50 (dashed) and 200 (solid) m y^{-1}
PIG
EKN
TG
120°W
140°W
Surface elevation (m)
0 250 500 750 1000 1250 1500 1750 2000

(b)

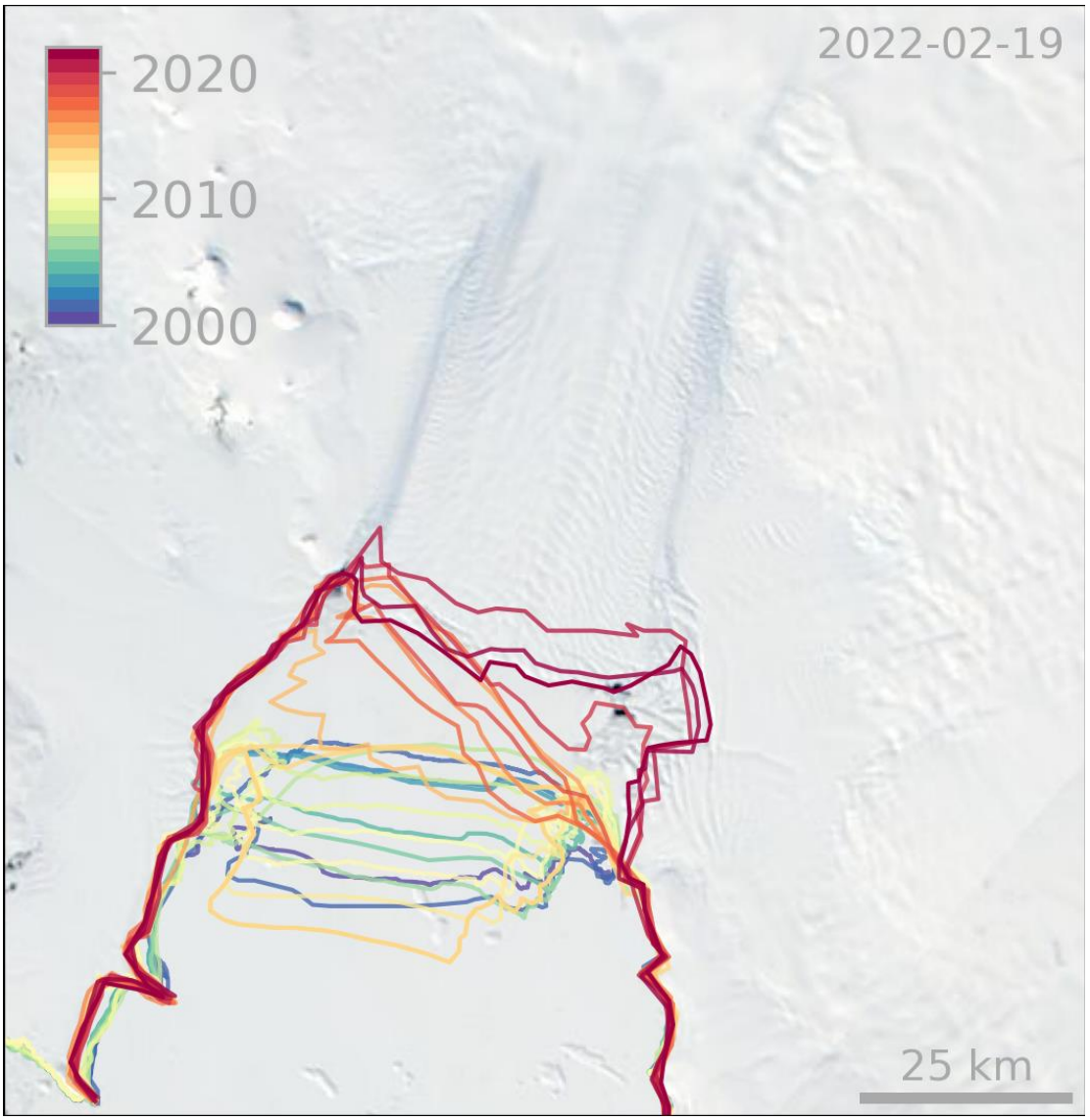

Figure 1: **Pine Island Glacier (PIG) and surroundings:** (a) Digital elevation map (DEM) at 1 km resolution, constructed using data for March 1994-January 1995 and February 2003-March 2008, showing PIG and the Thwaites Glacier (TG). The shading and the black contours show the surface elevation (m), contoured every 500 m and labelled every 1,000 m, while the regions where the ice velocity is equal to 50 m y^{-1} and 200 m y^{-1} are denoted by the dashed~~thin~~ and solid~~thick~~ cyan~~purple~~ contours, respectively. The ice velocities are estimated using data from the National Snow and Ice Data Center (NSIDC; Rignot et al., 2017) for 1996-2016. The blue line highlights the ice shelves borders. The solid red rectangle~~box~~ represents the domain over which the averaging is performed for the time series in Fig. 7 (-101.5ºW to -99.5ºW~~; and~~ -75.5ºS to -74.5ºS), whereas the dashed red rectangle highlights the domain used in Figs. 3-4 (105ºW to 95ºW; 80ºS to 70ºS). The location of the Evans Knoll weather station (-74.85ºS; -100.404ºW) is given by the green circle. (b) 19 February 2022 MODIS satellite image of PIG with an overlay of historical calving fronts since 2000.

The melting around PIG has been attributed mostly to basal melt and ocean-ice dynamics~~, in particular to the presence of relatively warm deep water on the Amundsen Sea continental shelf (Jacobs et al., 2011;) with the exposure of the grounded ice to the ocean water once the floating~~

ice retreats (Weber et al., 2017; De Rydt et al, 2021; Joughin et al., 2021). Calving events themselves can promote further ice loss through the associated ocean mixing that warms up deep water (Meredith et al., 2022). There is, however, considerable interannual variability, in line with changes in ocean currents and local wind stress (Webber et al., 2017). Other factors, such as changes in ice rheology and basal slipperiness (De Rydt et al., 2021), can also explain the recent ice loss at PIG. While ocean dynamics likely account for most of the observed ice loss, atmospheric forcing may also be important in modulating PIG ice loss, as is it has been shown recently to be the case elsewhere in the continent (e.g. Francis et al. 2021, 2022; Greene et al., 2022). Besides atmospheric rivers (Willie et al., 2019, 2021, 2022; Francis et al., 2020) and associated surface radiative warming, one of the meteorological phenomena that can foster ice damage around Antarctica is Foehn winds (Elvidge and Renfrew, 2016; Ghiz et al. 2021). The word Foehn, which means "hair dryer" in German, refers to the warm and dry winds that descend on the leeside of a mountain range. During Foehn events, anomalously warm and dry air masses occur in the lee slopes of a mountain range in response to orographic blocking of humid air upwind (Elvidge and Renfrew, 2016). Foehn effects can trigger surface melting and snow or ice sublimation (Bell et al., 2018), with melting less likely as the low humidities during Foehn episodes cause large latent heat losses from the snowpack and hence prevent its warming. Additionally, Foehn windseffects can promote the depletion of the firn air content at the top of the ice shelf with the resulting impermeable ice-surface encouraging meltwater-induced hydrofracture (Bell et al., 2018). Besides, Foehn winds can themselves promote ice breakup through the melting of snow (Bell et al., 2018) and the fostering of calving events (Miles et al., 2017), as an offshore wind direction, combined with ocean swells, aids in the breakup and subsequent drifting of newly formed icebergs (Francis et al., 2022).

Several studies have reported the occurrence of Foehn around Antarctica such as in the Ross Sea (e.g., Speirs et al., 2013; Zou et al. 2021a, b), PIG (Djoumna and Holland, 2021), Vestfold Hills in East Antarctica (Gehring et al., 2022) and Antarctic Peninsula (e.g., Laffin et al., 2021). Zou et al. (2021a, b) investigated the processes behind four major melting events at the Ross Ice Shelf. In three of the four cases Foehn warming occurred for more than 40% of the melting period, and the Foehn effect causeingd a 2-4ºC increase in surface temperature. The authors concluded that Foehn can be an important contributor to surface melting in Antarctica, which can increase the effects of warm and moist air advection. Djoumna and Holland (2021) reported Foehn conditions around PIG during March 2013 after the onset of a warm air intrusion associated with an atmospheric river. The combination of warm and moist air advection from lower latitudes and Foehn winds likely explains the record temperature of 17.5ºC observed at the northern tip of the Antarctic Peninsula on 24 March 2015 (Bozkurt et al., 2018). A region in Antarctica particularly prone to Foehn effects is the McMurdo Dry Valleys (Speirs et al., 2010): in the presence of a steep pressure gradient, with a ridge over Victoria Land and a low pressure over the Amundsen/Ross Sea, a warming of roughly 30ºC in just 3 h has been observed at the valley floor. Speirs et al. (2013) presented a 20-year climatology of Foehn events at this siteMcMurdo Dry Valleys from weather

station data. They reported positive trends for all seasons during 1999-2008 with a larger magnitude in winter when the large-scale dynamics favour the occurrence of Foehn. The role of Foehn winds in the disintegration and collapse of the Larsen ice shelves A, B and C on the Antarctic Peninsula in 1995, 2002 and 2017 respectively, has been widely reported (~~Cape et al. 2014, 2015;~~ Massom et al., 2018). In fact, during periods of strong westerlies, the warmer and more moist maritime air is forced to rise over the mountains in the western Antarctic Peninsula and warms and dries out on the leeside, generating frequent Foehn events over the ice shelves on the eastern side of the peninsula (Laffin et al., 2021). The complex terrain around PIG (Fig. 1a) favours Foehn wind occurrence there as well.

~~Laffin et al. (2021), and for the Antarctica Peninsula using a combination of model, surface observations and reanalysis data, found that the Foehn effect accounts for roughly 3% of the total surface melt. However, close to the mountains, this figure can rise to as much as 18%. The number of Foehn days, more so than its strength, explains the annual variability in melting triggered by the Foehn effects. Even though no statistically significant trend in Foehn occurrence is seen in the 1979-2018 period, an increased occurrence in the summer and decreased in the other three seasons is detected in 1999-2018. The same study noticed that Foehn days in the austral summer are positively correlated with the Southern Annular Mode (SAM, Marshall et al., 2003), an index which gives an indication of the strength and latitudinal position of the westerlies in the Southern Hemisphere, and negatively correlated with the SAM in the austral autumn. Positive SAM events also foster the occurrence of Foehn in the Antarctic Peninsula owing to the stronger westerly flow (Cape et al., 2015).~~

Despite major advances in the understanding of the Antarctic surface mass balance in recent decades, there are still major uncertainties (e.g. The IMBIE team, 2018) in particular in areas that are prone to ice loss such as PIG (Kowalewski et al., 2021). An important process for the surface mass balance is snow evaporation or sublimation (Das et al., 2013; Mottram et al., 2021), which is typically difficult to detect from observations given its nature. Even though Foehn events are believed to play an important role in the surface mass loss around Antarctica (Ghiz et al., 2021), the underlying processes remain unclear. Moreover, no study has examined the occurrence of Foehn on a longer time-scale over PIG, even though it is expected to have a significant impact given the steep topography in the region (Fig. 1a). Hence, it is vital to quantify the occurrence of Foehn episodes so as to better understand their role in ice loss through melting and/or sublimation. This is achieved in the present work, where the occurrence of Foehn at PIG and its role in the surface mass balance is investigated using a state-of-the-art reanalysis dataset, satellite imagery and in situ measurements.

The remainder of the paper is organised as follows. In section 2, the datasets used in this work as well as the Foehn-detection algorithm employed and how the different terms in the surface mass balance are quantified are described. Section 3 provides a discussion of the occurrence and trends

of Foehn over PIG, as well as its impacts on the surface mass balance. In Section 4 the focus is on the large-scale conditions that promote the occurrence of Foehn, while a case study in November 2011 is discussed in section 5. Section 6 summarises the main findings of the study.

2. Datasets and Methodology

2.1. Observational and Reanalysis Datasets

The main dataset used in this study is the ERA-5 reanalysis data (Hersbach et al., 2020), which is available on an hourly basis and on a 0.25º × 0.25º (~27 km) grid from 1950 to present. Both hourly pressure-level (Hersbach et al., 2018a) and surface (Hersbach et al., 2018b) data are considered in this work for the period 1980-2020. ERA-5 is one of the best performing reanalysis datasets around Antarctica in comparison with station observations as noted e.g. by Gossart et al. (2019).

The 1 km × 1 km dataset used for the Digital Elevation Model of Pine Island Glacier (PIG) and surrounding region combines measurements collected by the European Remote Sensing Satellite-1 (ERS-1) Satellite Radar Altimeter from March 1994 to January 1995, and the Ice, Cloud, and land Elevation Satellite (ICESat) Geosciences Laser Altimeter System from February 2003 to March 2008 (Bamber et al., 2009b). The ice velocity for PIG and Thwaites Glacier is estimated from a combination of satellite interferometric and synthetic-aperture radar systems, and is available at a 450 m spatial resolution from 1996 to 2016 (Rignot et al., 2016). Sentinel 2 satellite data, downloaded from Copernicus website (Copernicus, 2022), is used to extract the sea-ice front at PIG for 2000-2022.

Surface radiation fluxes from the Clouds and Earth's Radiant Energy System (CERES; Doelling et al. 2013, 2016) dataset are available on an hourly basis at 1º × 1º resolution from March 2000 to present. The CERES product used here is the SYN1deg - Level 3, which is freely available online (NASA/LARC/SD/ASDC, 2017), and is downloaded for the period 03-14 November 2011 that corresponds to the case study discussed in section 5.

10-min air temperature observations at the Evans Knoll station (-74.85ºS, -100.404ºW; 188 m above sea-level), located just to the northeast of PIG (green circle in Fig. 1a), are freely available at the Antarctic Meteorological Research Center & Automatic Weather Stations Project website, Space Science and Engineering Center, University of Wisconsin-Madison (Lazzara et al., 2022). This data is extracted for the case study (03-14 November 2011) considered in this work.

The surface melt area, for the period 03-14 November 2011, is estimated using measurements collected by the Moderate Resolution Imaging Spectroradiometer (MODIS; Kaufman et al.,

1997) on board the National Aeronautic and Space Administration's Terra and Aqua satellites. In particular, the daily global surface reflectance Level 3 data at 0.05º × 0.05º spatial resolution (MODIS products MOD09CMG and MYD09CMG for Terra and Aqua, respectively; Vermote 2015a,b) is downloaded, and the enhanced Normalised Difference Water Index (NDWI) defined in Moussavi et al. (2016) is estimated. The NDWI index makes use of the reflectance contrast between water and ice in the red (630-690 nm) and blue (450-510 nm) bands.

2.2. Foehn-Detection Algorithm

Foehn events at PIG are identified using a modified version of the algorithm proposed by Laffin et al. (2021), in which the authors studied Foehn episodes in the Antarctic Peninsula using ERA-5, model and observational data. A given hourly time-step is denoted as a Foehn time-step if the following three conditions hold:

$$\begin{cases} 2m\ Temperature > 60^{th}\ Percentile \\ 2m\ Relative\ Humidity < 30^{th}\ Percentile \\ 10m\ Wind\ Speed > 60^{th}\ Percentile \end{cases} \quad (1)$$

where the temperature, relative humidity (RH) and wind speed are extracted from ERA-5, and the algorithm is applied in a 10º × 10º domain (105º-95ºW, 80º-70ºS) centered on PIG. The thresholds are grid-point dependent, and while the RH and wind speed thresholds are computed over the full 40-year period (1980-2020), hourly thresholds for each month are used for the air temperature to account for the annual cycle. Laffin et al. (2021) used a threshold of 0ºC for the temperature as the focus was on Foehn events that cause surface melt. However, such a threshold is hardly met at PIG (Moncada and Holland, 2019; Djoumna and Holland, 2021) given its poleward location compared to the Antarctic Peninsula (~75ºS vs. ~60º-70ºS) and resulting reduced exposure to the warmer lower-latitude air. It is important to note, however, that a surface or air temperature above 0ºC is not needed for surface melting to take place. As noted by Ghiz et al. (2021), melting can occur at surface and air temperatures below freezing provided the melt energy, given by the sum of the surface radiation, turbulent and ground heat fluxes, is positive for at least two diurnal cycles. In addition to melting, Foehn promotes snow sublimation (Kirchgaessner et al., 2021) and depletes firn air content from ice shelves, which encourages meltwater-induced hydrofracture (Bell et al., 2018). Given this, the 60th percentile of the air temperature is used as the temperature threshold instead, in line with that considered for the wind speed but taking into account the strong annual variability in the region. The threshold values range from about 2 to 12 m s^{-1} for the 10-m wind speed, 232 K to 274 K for the 2-m air temperature, and 59 to 82% for the 2-m relative humidity.

It is important to note that ERA-5 reanalysis data lacks the spatial resolution to properly resolve smaller-scale flows, and therefore may not give a full picture of Foehn around PIG. However, the findings of Laffin et al. (2021) suggest that its representation of Foehn, at least in

the Antarctic Peninsula, is accurate enough in particular for moderate and strong episodes to justify its use here. In particular, these authors found that the reanalysis captured roughly 92% of the Foehn events detected with in situ weather station data. The biases in the ERA-5 radiative fluxes, which in a comparison with in situ observations at Siple Dome next to the Ross Ice Shelf are as large as 100 $W m^{-2}$ for the downward shortwave and 50 $W m^{-2}$ for the downward longwave (Ghiz et al., 2021), suggest that a Foehn identification algorithm based on the surface energy budget, and using ERA-5 data, may not be optimal for Antarctica. The reanalysis performance in terms of 2-m temperature, relative humidity and 10-m wind speed, the fields used in the Foehn detection algorithm (1), is superior, with typical biases of 0.5-1.5ºC, 5-10% and 0.5-1.5 $m s^{-1}$, respectively, as noted by Gossart et al. (2019).

2.3. Surface Mass Balance

Over snowy regions such as Antarctica, and following Dery and Yau (1999, 2002) and Scarchilli et al. (2010), the surface mass balance can be expressed as

$$S = P - E - M - Q_{snow} - D \quad (2)$$

where S is the rate of accumulation or storage of snow at the surface, P is the precipitation (snowfall) rate, E is the surface evaporation rate which includes the sublimation rate (Q_{surf}), M represents the surface melt and runoff rate, Q_{snow} is the blowing snow sublimation rate and D is the blowing snow divergence rate. All terms are expressed as mm of water equivalent per day (mm w.e. day^{-1}).

In ERA-5, snow is regarded as an additional layer on top of the soil layer, and is characterized by a snow temperature T_{sn}, with independent and prognostic thermal and mass contents. Snow melting takes place if T_{sn} exceeds the melting point (273.16 K), while snow sublimation is estimated with the bulk aerodynamic formula using the wind speed and specific humidity of the lowest model layer and the saturated specific humidity at T_{sn} (ECMWF, 2016). The bulk aerodynamic formula, used in ERA-5, performed well in estimating the observed snow sublimation over the Himalayas (Stitger et al., 2018), but has not been evaluated over Antarctica. What is more, blowing snow is not accounted for in the reanalysis dataset, which is problematic as during Foehn events it is known to lower the albedo and increase surface compaction, and hence enhance the effects of Foehn on the snowpack (e.g. Bromwich, 1989; Scarchilli et al., 2010; MacDonald et al., 2018; Datta et al., 2019; Pradhananga and Pomeroy, 2022). As a result, the terms Q_{surf}, D and Q_{snow} in Eq. (2) are estimated as detailed below, while P and M are taken directly from the reanalysis. The ERA-5 predicted surface mass anomaly, given by precipitation minus sublimation with the monthly mass accumulation over the period 1980-2001 removed, over the Dronning Maud Land in East Antarctica for 2006-2017 compares well with that estimated from the measurements collected by the Gravity Recovery

and Climate Experiment satellite (Gossart et al., 2019). In fact, ERA-5 is the best performing reanalysis product out of those considered, closely following the satellite-derived estimates, with a mean absolute error of 24 Gt yr^{-1}. This justifies the use of the reanalysis' P and M in this work. All constants are defined in Table 1.

The surface sublimation rate, Q_{surf}, included in the term E in Eq. (2), is parameterized as

$$Q_{surf} = \rho' \frac{\rho_{air}\overline{(w'q')}}{\rho_{water}} = \rho' \frac{\rho_{air}(u_* q_*)}{\rho_{water}} \quad (3)$$

with

$$u_* = \frac{\kappa U}{ln\, ln\left(\frac{z + z_0}{z_0}\right)}$$

$$q_* = \frac{\kappa q_{si}(RH_{ice} - 1)}{ln\, ln\left(\frac{z + z_q}{z_q}\right)}$$

where u_* is the friction velocity, q_* is a humidity scale, κ is the von Karman constant, U is the wind speed at height z above the surface (taken to be 10-m), z_0 is the aerodynamic roughness length, q_{si} is the saturation mixing ratio over ice, RH_{ice} is the relative humidity with respect to ice, z_q is the roughness length for moisture over snow (taken to be the same as z_0), ρ is the air density, ρ_{water} is the density of water, and ρ' is a conversion factor from m s^{-1} to mm day^{-1}. If $RH_{ice} > 1$, q_* becomes positive and deposition to the surface is said to occur. The term $\overline{(w'q')}$ is the turbulent moisture flux at the surface, with $\rho_{air}\overline{(w'q')}$ giving the sublimation rate (van den Broeke, 1997). The rate of water equivalent lost to sublimation is obtained by dividing the sublimation rate by the density of water, as done by Montesi et al. (2004).

The blowing snow sublimation rate, Q_{snow}, is expressed as in Eq. (4) below

$$Q_{snow} = \frac{a_0 + a_1\xi + a_2\xi^2 + a_3\xi^3 + a_4 U_{10} + a_5\xi U_{10} + a_6\xi^2 U_{10} + a_7 U_{10}^2 + a_8\xi U_{10}^2 + a_9 U_{10}^3}{U'} \quad (4)$$

with

$$\xi = \frac{RH_{ice} - 1}{2\rho_{ice}[F_k(T) + F_d(T)]}$$

$$U' = \frac{\left(1 - \frac{U_t}{U_{10}}\right)^{2.59}}{\left(1 - \frac{6.975}{U_{10}}\right)^{2.59}}$$

$$U_t = 6.975 + 0.0033\,(T_{2m} + 27.27)^2$$

where ξ is a thermodynamic term, U_{10} is the 10-m wind speed, U' is a non-dimensional factor that removes the dependence on the saltation mixing ratio, U_t is the threshold for initiation of blowing snow, T_{2m} is the 2-m temperature, ρ_{ice} is the density of ice, and $F_k(T)$ and $F_d(T)$ are the conductivity and diffusion terms associated with sublimation, both temperature dependent and extracted from Rogers and Yau (1989). While negative values of Q_{surf} indicate sublimation and positive values denote deposition, the opposite is true for Q_{snow}, with positive values implying sublimation of blowing snow is taking place.

The snow transport rate, Q_t, is a vector quantity whose magnitude is given by

$$Q_t = BU_{10}^C \quad (5)$$

with the direction obtained by projecting it onto the 10-m horizontal wind vector. The divergence term D in Eq. (2) is then obtained by

$$D = \frac{\rho'}{\rho_{water}} \nabla \cdot Q_t \quad (6)$$

Constant	Value	Constant	Value
a_0	3.78407×10^{-1}	a_8	1.56862×10^{-3}
a_1	-8.64089×10^{-2}	a_9	-2.93002×10^{-4}
a_2	-1.60570×10^{-2}	κ	0.4
a_3	7.25516×10^{-4}	ρ'	8.6400×10^{7}
a_4	-1.25650×10^{-1}	ρ_{water}	1000 kg m^{-3}
a_5	2.48430×10^{-2}	ρ_{ice}	917 kg m^{-3}
a_6	-9.56871×10^{-4}	B	2.2×10^{-6} kg m$^{-5.04}$ s$^{3.04}$
a_7	1.24600×10^{-2}	C	4.04

Table 1: Constants used in the surface mass balance.

3. Foehn Events at PIG and Impacts on Ice

The statistics of Foehn events at PIG are summarized in Fig. 2. Foehn is more frequent in the austral winter season, in particular from June to October, and less common in the summer albeit with a considerable spread in all months (Fig. 2a). The annual cycle in the duration of Foehn events is less pronounced, with monthly-mean values in the range 5 to 9 h, with August featuring both the highest number (~123) and longest (~9 h) Foehn episodes. At the Antarctic Peninsula, Foehn occurrence peaks in the transition seasons (Wiesenekker et al., 2018; Laffin et al., 2021) whereas at the McMurdo Dry Valleys located next to the Ross Sea it is more frequent in winter (Speirs et al., 2013). As Foehn events are driven by large-scale pressure gradients, the difference in the timing of the peaks is likely a result of the variability in the position of the baroclinic systems. In particular, and as noted by Simmonds et al. (2003), the cyclonic activity in the Ross Sea, northern Antarctic Peninsula and around PIG is maximized in winter whereas in the central Antarctic Peninsula it is the highest in the summer. Consistent with this, in the Amundsen and Bellingshausen Seas there is a pronounced equatorward shift in the mid-latitude storm track in the summer months (Dias da Silva et al., 2021), which is in line with the higher occurrence of Foehn at PIG in the colder months. The Amundsen Sea Low (ASL), a semi-permanent low pressure in the Amundsen-Bellingshausen Seas (60º-75ºS and 170º-290ºE) that exhibits the largest geopotential height variability in the Southern Hemisphere, is likely to play a major role in the occurrence of Foehn at PIG (Mclennan and Lenaerts, 2021). Meridionally, it is at its most poleward location in late winter and is shifted further equatorwards in the summer, while longitudinally it is the closest to PIG in the summer months (Raphael et al., 2016). As Foehn is more likely when the ASL is just to north of PIG with its clockwise circulation encouraging Foehn effects in the region, as noted in section 4, the intricate annual cycle of the ASL may explain the highest Foehn occurrence in late winter and why it still takes place in the summer months. In the area around PIG, there are on average 3.0 Foehn days in the month of August (123 occurrences over the 41-year period 1980-2020) lasting roughly 7.9 h each, whereas in January there are 0.37 Foehn days per month that typically last for about 5.1 h. Wiesenekker et al. (2018) reported an average of 1.3 to 5.8 Foehn events per month in the Antarctic Peninsula over 1979-2016, with roughly 70-80% of the events in December 2014 - December 2016 lasting less than a day. These figures are higher than those at PIG shown in Fig. 2a, which is due to the fact that the Antarctic Peninsula is more exposed to the mid-latitude storm track, with the higher terrain on its western side promoting Foehn effects.

Fig. 2b gives the area-averaged air temperature and sensible heat flux for the Foehn events, with the air temperature, sensible heat flux and RH anomalies during Foehn episodes plotted in Fig. 2c. The sensible heat flux is positive, and hence directed downwards towards the surface, with monthly-mean values in the range 18 to 42 $W m^{-2}$, with higher values in the winter months. This is in line with Laffin et al. (2021) and with the fact that the sensible heat flux around Antarctica is maximized in the colder months when the surface to air temperature gradient is the highest, owing to the sharp thermal inversions that develop at this time of the year (Reijmer et al., 1999). The

magnitude of the fluxes is comparable to that modeled over the Antarctica Peninsula (e.g. Elvidge et al., 2014) and at Joyce Glacier in McMurdo Dry Valleys (Hofsteenge et al., 2022). The air temperature during Foehn events at PIG is below freezing, ranging from -7ºC in January to -22ºC in August. However, melting and sublimation can still occur, in particular when accounting for the large variability which is maximized in the summer (e.g., Ghiz et al. 2021). Fig. 2c shows that Foehn effects lead to generally warmer (air temperatures anomalies typically of +0-7ºC) and drier (RH anomalies in the range -8% to -11%) weather conditions accompanied with a downward sensible heat flux (anomalies of +14-21 $W\,m^{-2}$).

Fig. 2d gives the trends in the number of Foehn days and in the duration of Foehn events for 1980-2020, both of which are not statistically significant. When the analysis is extended to individual seasons, only one statistically significant trend is found, that of the duration for the autumn season, with a slope of about -0.002 days yr^{-1} (not shown). ~~A positive trend is present in the former even though the slope, of ~0.1 days year^{-1}, is not statistically significant at the 95% confidence level, while the trend in the duration of Foehn events is negligible. An inspection of the trends for individual seasons revealed that only the one in the duration of Foehn events for the autumn season is statistically significant, with a slope of about -0.002 days year^{-1} (not shown).~~ Studies of trends of Foehn occurrence in Antarctica also reported non statistically significant slopes, in particular over the two major studied regions of the McMurdo Dry Valleys (e.g., Speirs et al., 2013) and the Antarctic Peninsula (e.g., Laffin et al., 2021). ~~However, Cape et al. (2015), and for a single long-term station to the north of the Larsen C Ice Shelf east of the Antarctic Peninsula, found a positive trend in the summer months of about 1.46% year^{-1} for the period 1962-2010 statistically significant at the 95% confidence level.~~ Fig. 2d also shows considerable inter-annual variability in both the number and duration of Foehn days. The major peaks taking place mostly in La Nina (1984, 1985, 1999, 2010) or neutral (1981, 1993, 1996, 1999, 2003, 2008, 2013) years, while the minimum in 1982, 1986, 1997 and 2015 coincide with El Nino years (Lestari and Koh, 2016; Zhang et al., 2022). In La Nina conditions, the ASL is more active than normal (Raphael et al., 2016), which may promote the occurrence of Foehn, while in El Nino episodes the presence of a ridge over the Amundsen and Bellingshausen Seas (Yuan, 2004) may discourage Foehn effects at PIG. A discussion of the large-scale patterns that favor Foehn occurrence at PIG is given in section 4.

(a) (b)

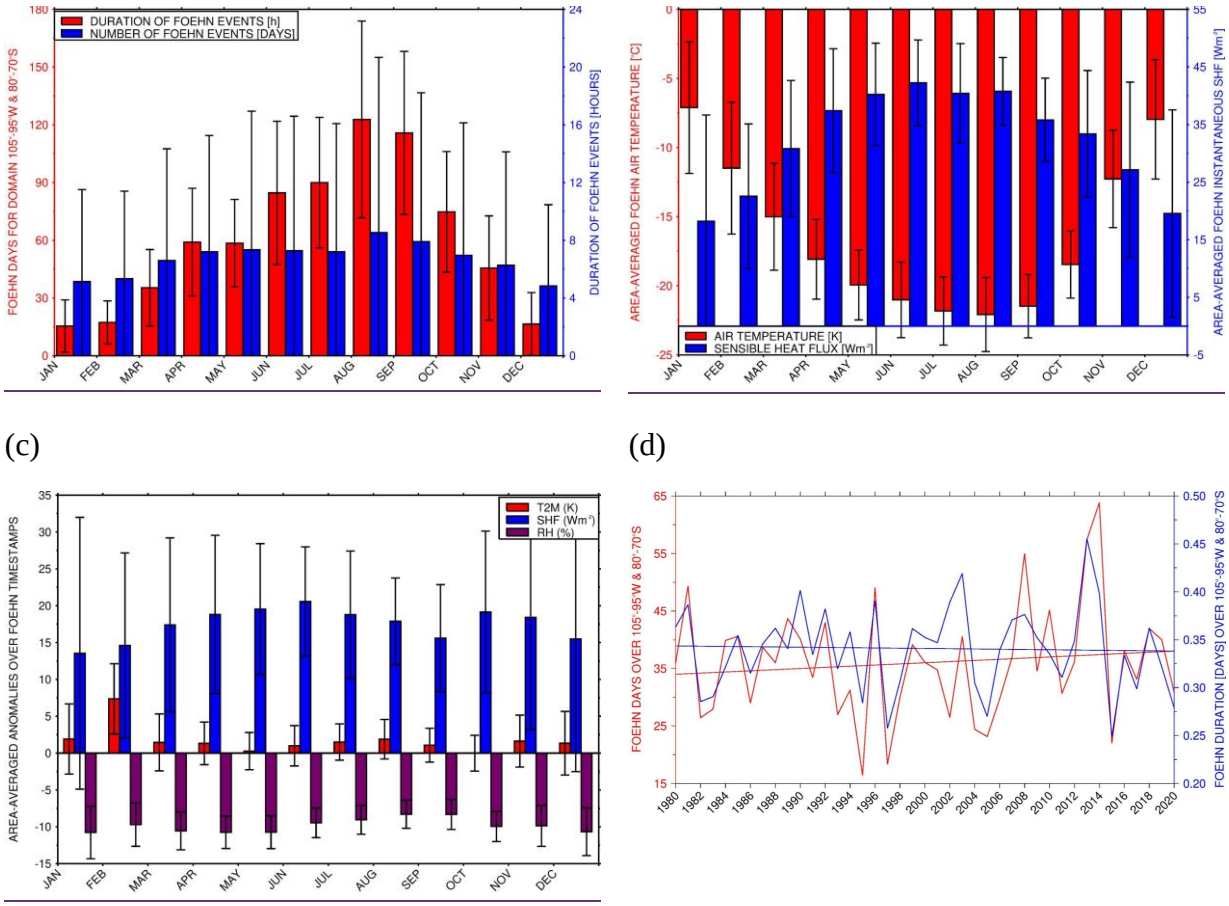

Figure 2: **Climatology and trends of Foehn events:** (a) Monthly mean (histogram bars) and standard deviation (error bars) of Foehn days (orange; left axis) and duration of Foehn events (hours; blue; right axis) for the period 1980-2020 and for the domain 95ºW-105ºW and 80ºS-70ºS. (b) is as (a) but for the area-averaged air temperature (ºC; orange; left axis) and instantaneous sensible heat flux (W m^{-2}; blue; right axis; positive if downwards towards the surface). (c) gives the air temperature (ºC; orange), instantaneous sensible heat flux (W m^{-2}; blue) and relative humidity (%; purple) anomalies during Foehn timestamps. (d) Trend in Foehn days (left; red) and in the duration of Foehn events (right; blue) for 1980-2020. The slopes of the Foehn days and duration are 0.101024 days yr^{-1} and -0.0001 days yr^{-1} with a statistical significance of 55% and 18%, respectively.

~~(a)~~

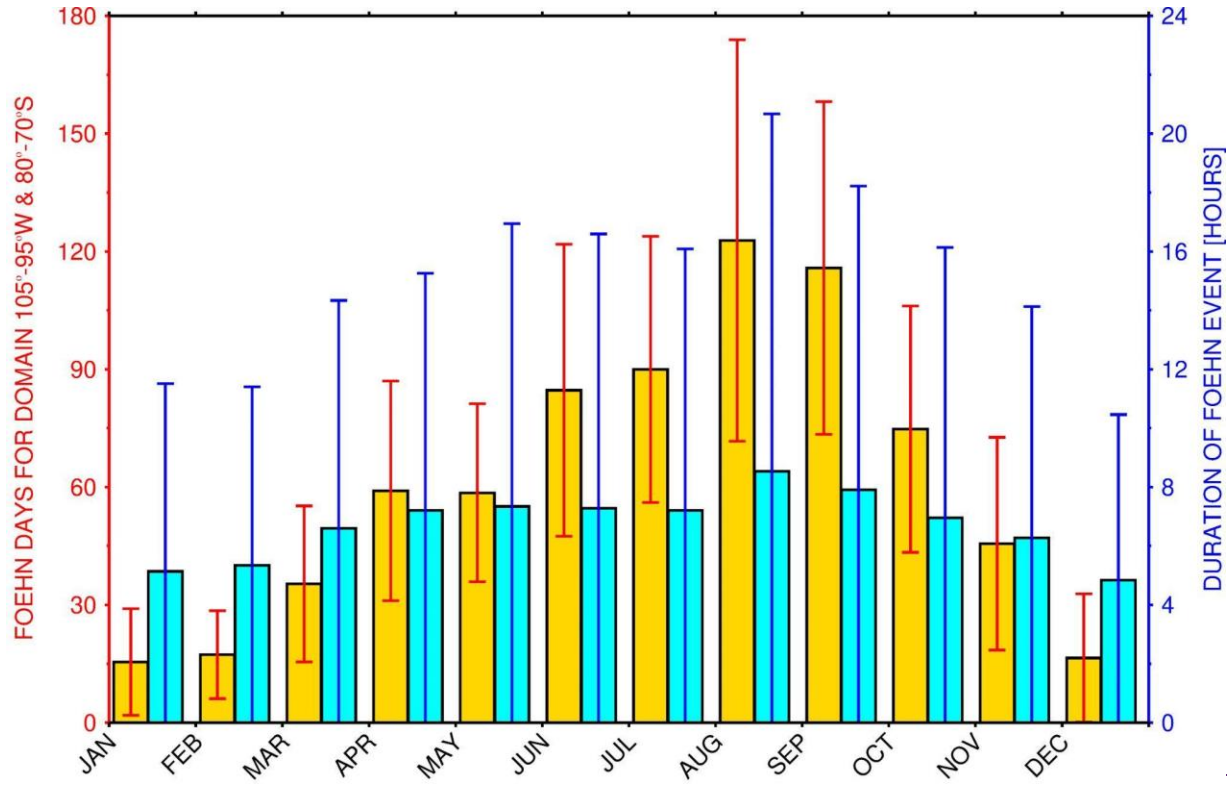
FOEHN DAYS FOR DOMAIN 105°-95°W & 80°-70°S
DURATION OF FOEHN EVENT [HOURS]
0
30
60
90
120
150
180
0
4
8
12
16
20
24
JAN
FEB
MAR
APR
MAY
JUN
JUL
AUG
SEP
OCT
NOV
DEC

~~(b)~~

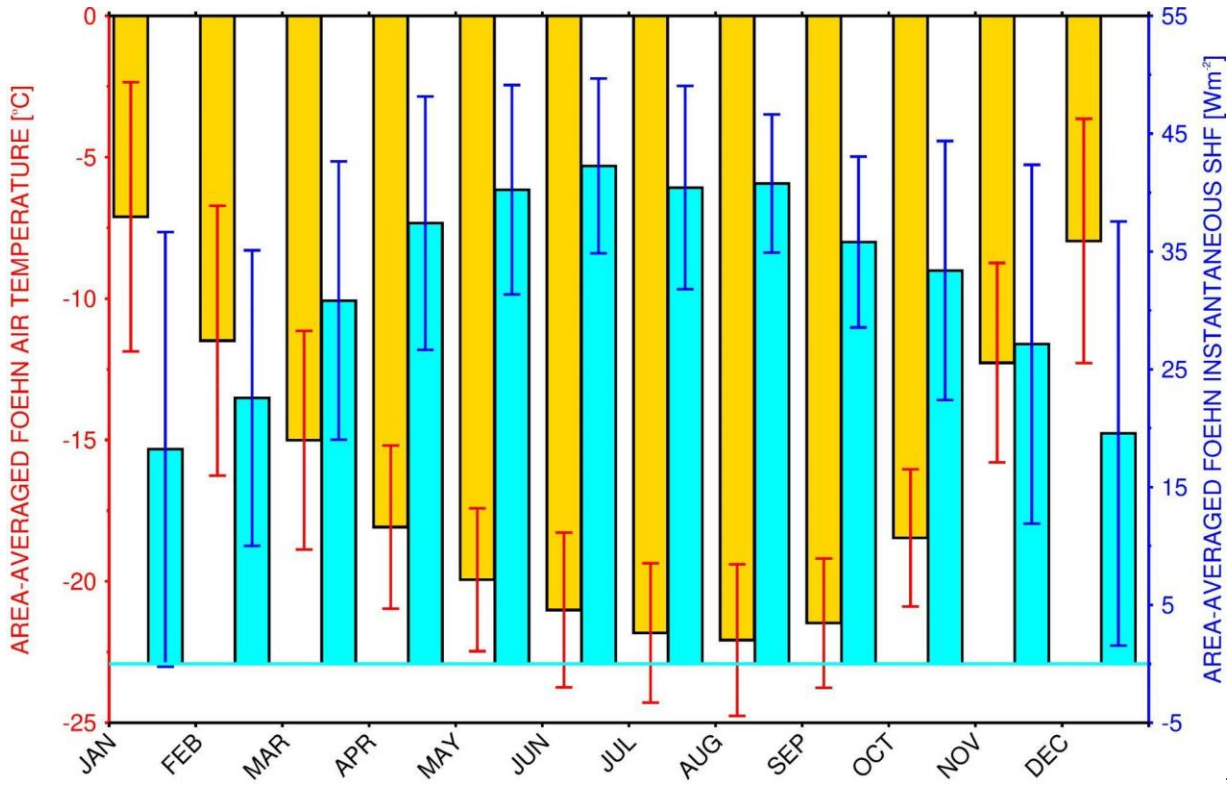
AREA-AVERAGED FOEHN AIR TEMPERATURE [°C]
AREA-AVERAGED FOEHN INSTANTANEOUS SHF [Wm-2]
0
-5
-10
-15
-20
-25
55
45
35
25
15
5
-5
JAN
FEB
MAR
APR
MAY
JUN
JUL
AUG
SEP
OCT
NOV
DEC

~~(c)~~

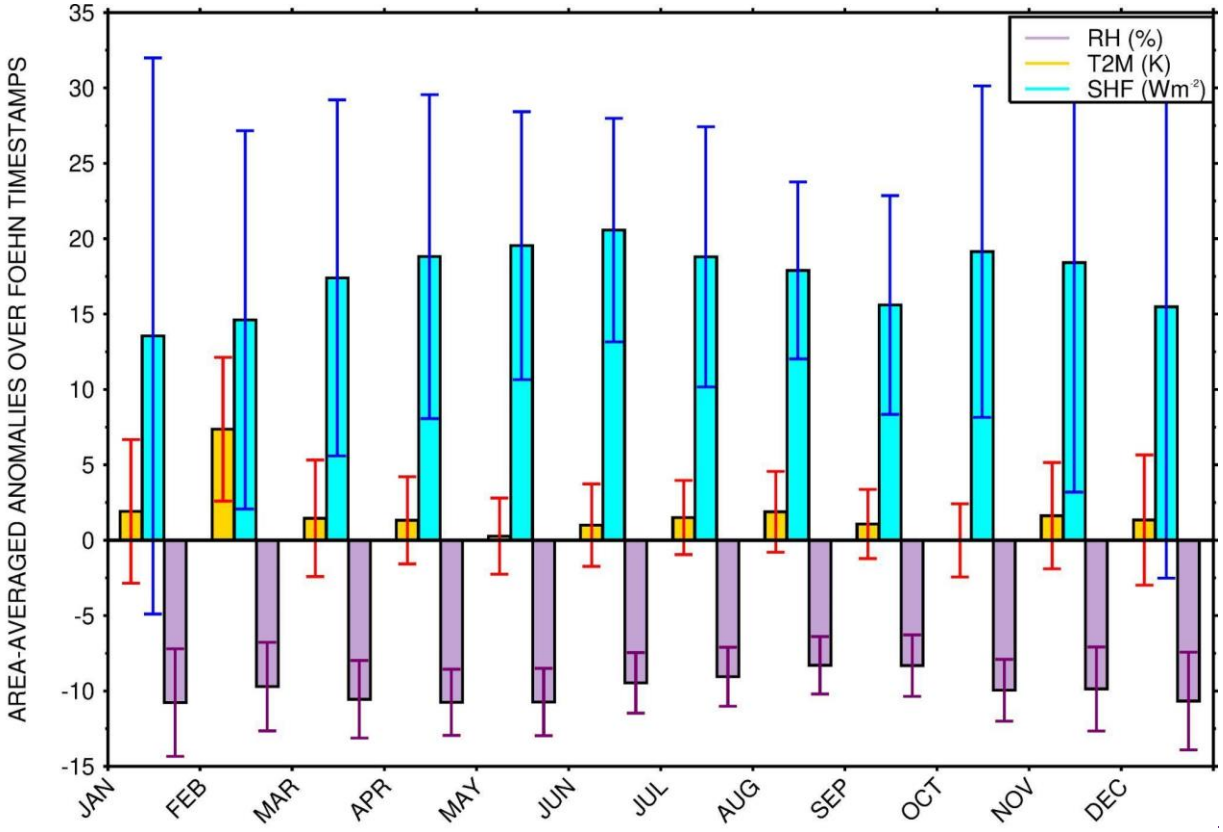
AREA-AVERAGED ANOMALIES OVER FOEHN TIMESTAMPS
RH (%)
T2M (K)
SHF (Wm-2)
35
30
25
20
15
10
5
0
-5
-10
-15
JAN
FEB
MAR
APR
MAY
JUN
JUL
AUG
SEP
OCT
NOV
DEC

~~(d)~~

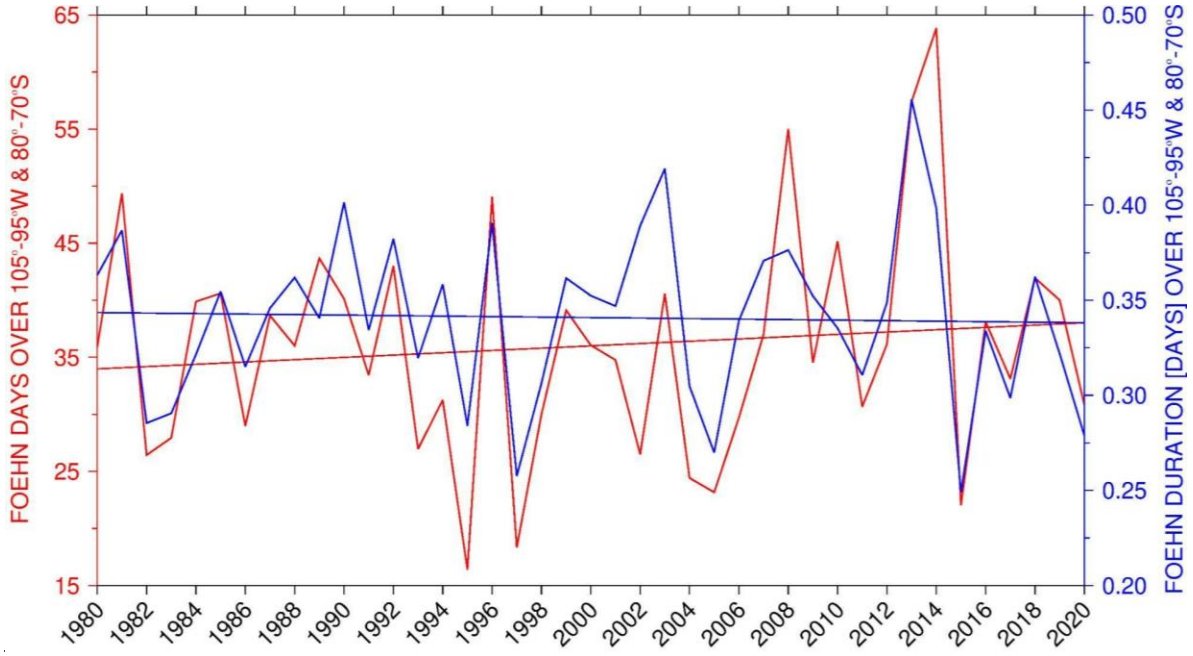
FOEHN DAYS OVER 105°-95°W & 80°-70°S
FOEHN DURATION [DAYS] OVER 105°-95°W & 80°-70°S
65
55
45
35
25
15
0.50
0.45
0.40
0.35
0.30
0.25
0.20
1980
1982
1984
1986
1988
1990
1992
1994
1996
1998
2000
2002
2004
2006
2008
2010
2012
2014
2016
2018
2020

Figure 2: Climatology and trends of Foehn events: (a) Monthly mean (histogram bars) and standard deviation (error bars) of Foehn days (orange; left axis) and duration of Foehn events (hours; blue; right axis) for the period 1980-2020 and for the domain 95ºW-105ºW and 80ºS-70ºS. (b) is as (a) but for the area-averaged air temperature (ºC; orange; left axis) and instantaneous sensible heat flux ($W.m^{-2}$; blue; right axis; positive if downwards towards the surface). (c) gives the air temperature (ºC; orange), instantaneous sensible heat flux ($W.m^{-2}$; blue) and relative humidity (%; purple) anomalies during Foehn timestamps. (d) Trend in Foehn days (left; red) and in the duration of Foehn events (right; blue) for 1980-2020. The slopes of the Foehn days and duration are 0.101024 $days.yr^{-1}$ and -0.0001 $days.yr^{-1}$ with a statistical significance of 55% and 18%, respectively.

A quantification of the potential for surface melting and sublimation is presented in Fig. 3. The "melt potential" index (MPI) is defined following Orr et al. (2022) using the daily maximum air temperature for 1980-2020, for both the full year and extended summer season (November to February, NDJF). At each grid-point, the MPI intensity is given by the difference between the 95th percentile of the daily maximum air temperature distribution for the Foehn/no-Foehn days and the melt threshold of 273.15 K, while the MPI frequency is the percentage of values higher than the threshold. The "sublimation potential" index (SPI) is defined in the same way but using the 95th percentile of the daily maximum of the hourly surface sublimation given by Eq. (3) and a threshold of zero, while its frequency expresses the percentage of the Foehn/no-Foehn days in the 1980-2020 period when there is sublimation for at least one hour per day at the site. Here, the difference between Foehn and no-Foehn timestamps is plotted for both indices to give insight into the effects of Foehn in surface melting and sublimation.

Surface melting is less common at PIG during Foehn events, with a MPI intensity and frequency reductions of about -1.3 K and -3%, respectively, with comparable values in NDJF (-0.9 K and -6%). This is expected, as the downward sensible heat flux is largely offset by the upward latent heat flux that arises from the drier near-surface air, making it harder for the snowpack to melt. Surface melting is confined to lower elevations where the temperature is higher. Here, there is also increasing exposure to the warmer and more moist maritime air masses compared to the high terrain inland. The fact that surface melting is more frequent in the adjacent Southern Ocean in Foehn episodes may be attributed both to the increased adiabatic compression of the winds as they descend towards the coastal regions, and the likely presence of a low pressure system north of the site during the Foehn events, as will be discussed in section 4. When all days (Foehn and no-Foehn) in 1980-2020 are considered, the MPI intensity and frequency at PIG for the full year are -0.27 K and 4%, respectively, and +0.87 K and 10% for NDJF (not shown). Orr et al. (2022), and using used higher spatial resolution (~12 km) modelling products over December-February 1979-2019 and for the whole Antarctica, to obtained values at PIG of 1.3-1.7 K and 23.7-23.8%. The MPI intensity and frequency difference between Foehn and no-Foehn days given in Figs. 3a-b stress the role of Foehn in discouraging surface melting at and around the glacier. Figs. 3c-d are as Figs. 3a-b but for the SPI. The seasonal variability is much reduced compared to that of the MPI, with an intensity difference between Foehn and no-Foehn days of +1.8 mm w.e. day^{-1} for the full year and +1.6 mm w.e. day^{-1} for NDJF, and a rather small change in frequency (<0.3%). When

all days are taken, the intensity ~~Surface sublimation at PIG is also more likely in the summer months, albeit the differences between the full year and NDJF are small, with~~ magnitudes are of about 3.34 and 3.39 mm w.e. day^{-1}, respectively, and a frequency of occurrence around 100% (not shown). The fact that the frequency is very high indicates that the daily maximum in the surface sublimation is positive nearly all the time at PIG, suggesting that there is at least 1 h of sublimation every day of the year for the 41-year period~~it is a regular occurrence~~ at the site. This also explains why there is hardly any change in frequency between Foehn and no-Foehn days. The SPI intensity, on the other hand, is roughly 50% larger during Fohn episodes, highlighting the role of Foehn effects in the surface sublimation. ~~Surface sublimation increases with the wind speed and air temperature, in line with the way it is parameterized, Eq. (3).~~ It is interesting to note that, e~~E~~ven though the near-surface wind in the region is stronger in the colder months ~~(cf. Figs. 3c-d)~~, the effects of Foehn on the 10-m wind in NDJF are largely similar to that in the full year (cf. Figs. 3c-d). ~~higher air temperatures in the summer decrease the supersaturation with respect to ice and hence promote the occurrence of sublimation. Windier and drier conditions, seen in Foehn events (Fig. 2c), also encourage surface sublimation.~~ The convergence of the near-surface wind in the PIG basin and the lower heights and consequently higher temperatures explain the maximum in surface sublimation in the region seen in Figs. 3c-d.

(a)

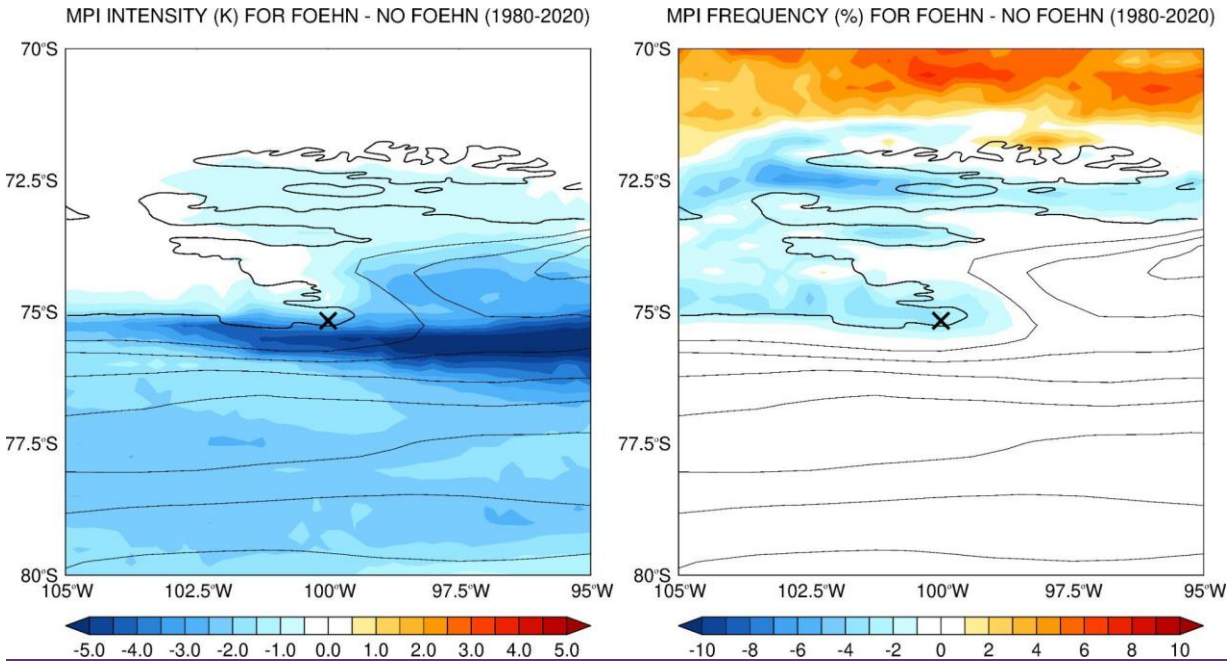

(b)

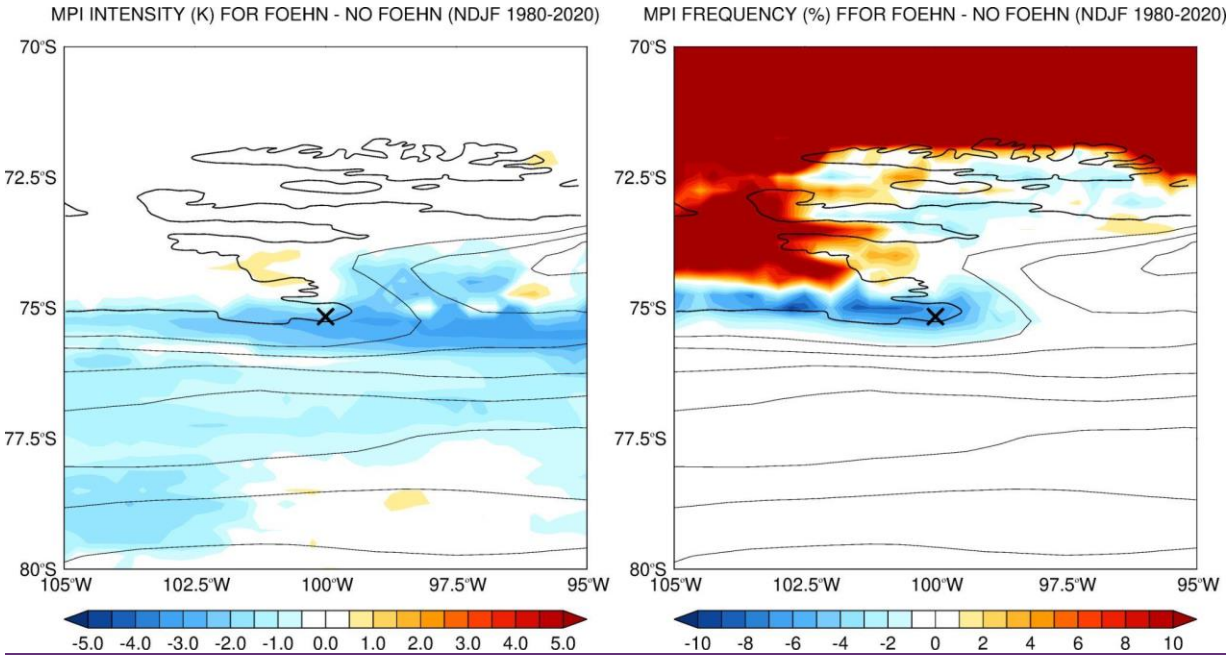
MPI INTENSITY (K) FOR FOEHN - NO FOEHN (NDJF 1980-2020)
MPI FREQUENCY (%) FFOR FOEHN - NO FOEHN (NDJF 1980-2020)
70°S
72.5°S
75°S
77.5°S
80°S
105°W
102.5°W
100°W
97.5°W
95°W
-5.0 -4.0 -3.0 -2.0 -1.0 0.0 1.0 2.0 3.0 4.0 5.0
-10 -8 -6 -4 -2 0 2 4 6 8 10

(c)

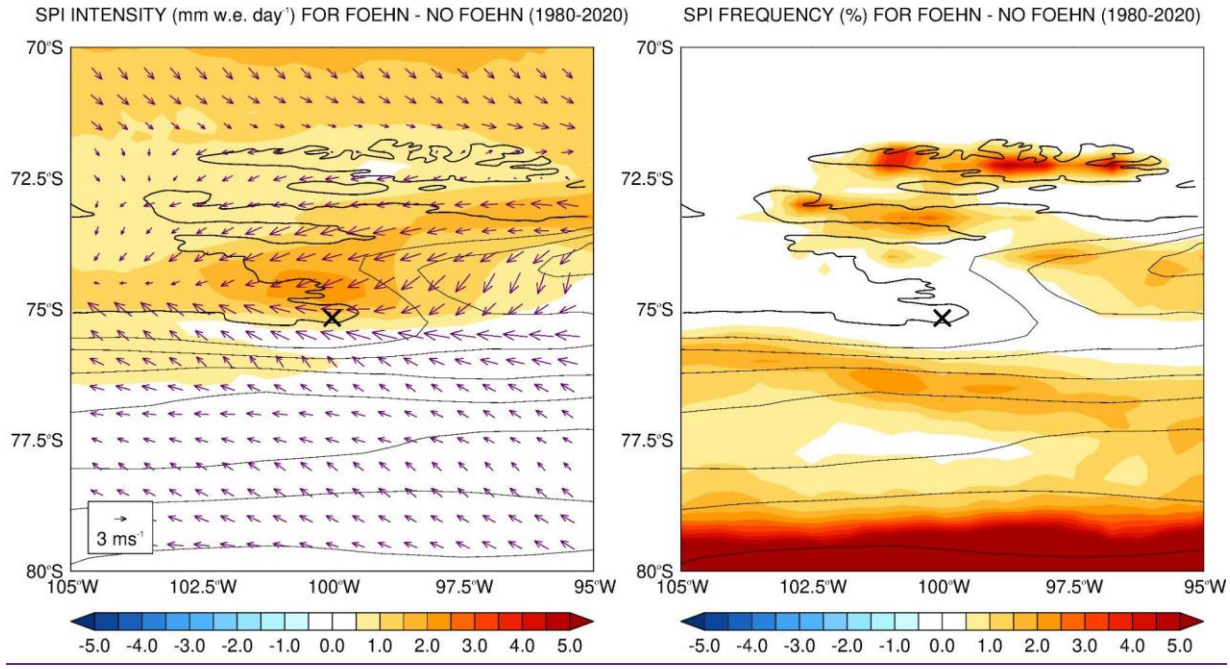
SPI INTENSITY (mm w.e. day⁻¹) FOR FOEHN - NO FOEHN (1980-2020)
SPI FREQUENCY (%) FOR FOEHN - NO FOEHN (1980-2020)
70°S
72.5°S
75°S
77.5°S
80°S
105°W
102.5°W
100°W
97.5°W
95°W
3 ms⁻¹
-5.0 -4.0 -3.0 -2.0 -1.0 0.0 1.0 2.0 3.0 4.0 5.0

(d)

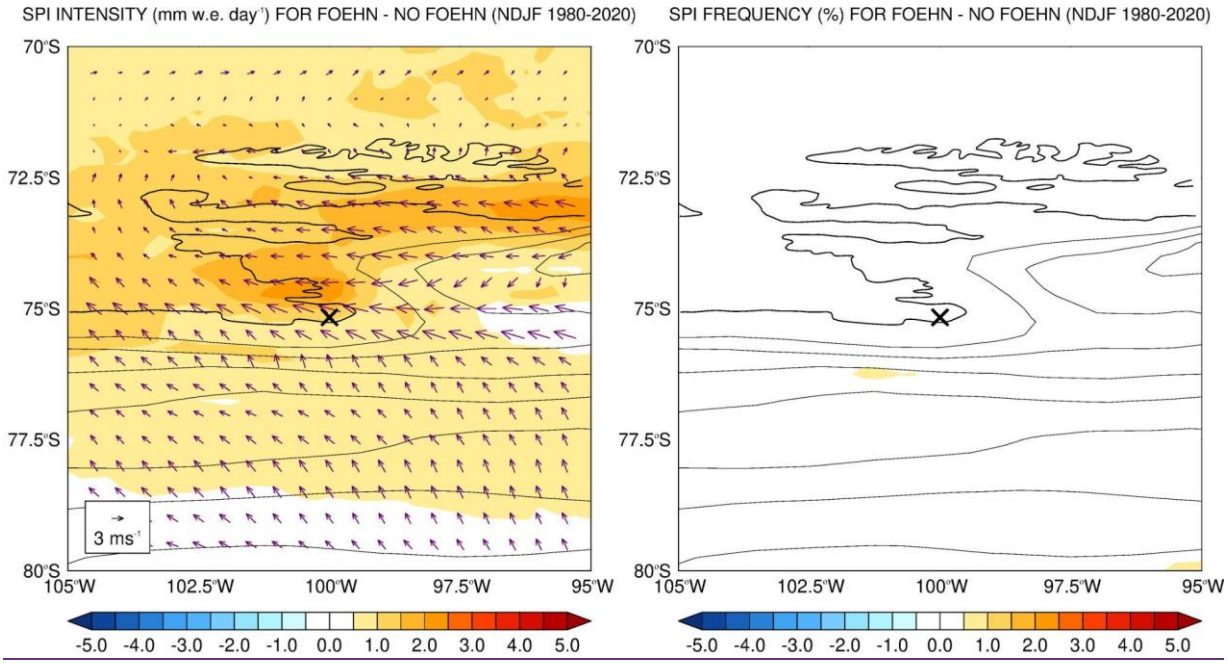

Figure 3: **Melt and Sublimation Potential Indices:** (a) "Melt Potential" index (MPI) intensity (K; left) and frequency (%; right), defined following Orr et al. (2022), for the difference between Foehn and no-Foehn timestamps for 1980-2020. The thin black lines are 250 m orography contours and the land-sea mask is represented by the thick black line. The cross gives PIG location (100ºW, 75º10'S). (b) is as (a) but for November-February (NDJF) only. (c)-(d) are as (a)-(b) but for the "Sublimation Potential" index (SPI), with the intensity given in mm of water equivalent per day (mm w.e. day^{-1}). The averaged 10-m horizontal wind vectors are drawn as arrows in the left panels of (c)-(d) for the respective period.

In order to explore the contribution of Foehn to the surface mass balance, Figs. 4a-f show the composite difference of the terms in Eq. (2) between Foehn and no-Foehn timestamps for 1980-2020. The Foehn minus no-Foehn values of the rate of accumulation or storage of snow at the surface (S), precipitation (snowfall) rate (P), surface melt and runoff rate (M), surface sublimation rate (Q_{surf}), blowing snow sublimation rate (Q_{snow}) and blowing snow divergence rate (D) at PIG are $S \sim$ -1.411, $P \sim$ -0.345, $M \sim$ -0.005, $Q_{surf} \sim$ -1.434, $Q_{snow} \sim$ 0 and $D \sim$ -0.363 mm w.e. day^{-1}, respectively. This indicates that (i) surface sublimation plays the dominant role in the surface mass balance during Foehn events (note that negative values of the surface sublimation rate, Q_{surf}, and positive values of the blowing snow sublimation rate, Q_{snow}, indicate sublimation); (ii) the sum of the two blowing snow terms, Q_{snow} and D, has a magnitude comparable to that of the precipitation/snowfall, P, roughly 25% smaller than that of the surface evaporation, but with the opposite sign in Eq. (2), reflecting a lack of snowfall during Foehn episodes due to the drier conditions while the convergence of blowing snow at the glacier basin adds to the surface mass; (iii) snow melting, M, makes a negligible contribution to the surface mass balance, being roughly three orders of magnitude smaller than the surface sublimation.

The surface sublimation rate (Fig. 4c) is considerable, with the values at PIG comparable to the maximum rates at a site in northern Victoria Land during November 2018 (Ponti et al., 2021), ~~four times larger than that estimated just off East Antarctica in late winter 2007 (Toyota et al., 2011), but smaller than those at individual events at the Princess Elizabeth base in East Antarctica (Gorodetskaya et al., 2015). The magnitude of the surface sublimation rate during Foehn events is~~ but roughly an order of magnitude smaller than that due to melting resulting from ice dynamics around Antarctica, including at PIG ~~at the Ronne Ice Shelf in the Weddell Sea~~ (Holland et al., 2007~~;~~), ~~Totten Ice Shelf in East Antarctica (~~ Rintoul et al., 2016~~;~~), ~~and at PIG and Thwaites Glacier in West Antarctica (~~ Feldmann et al., 2019). ~~Yang et al. (2010) compared the surface sublimation given by Eq. (3) with that estimated from a mesoscale model over the Arctic. They found that, for the boreal winter of 2006/2007, the spatial pattern was similar but the magnitude of the sublimation given by the model was larger than that estimated from the empirical formula. The coarse resolution of the ERA-5 data may lead to an underprediction of the strength of the near-surface wind and hence an underestimation of the surface sublimation. As noted before, the surface sublimation increases with the air temperature and wind speed, with both larger at PIG which explains the local maximum at the glacier basin.~~ Surface melting is negligible and confined to the coastal regions further north (Fig. 4d). As noted by Scarchilli et al. (2010), and in line with our findings (Figs. 4e-f), blowing snow plays an important role in the surface mass balance during strong wind (here Foehn) episodes. The magnitude of the total blowing snow sublimation and transport reported in that study, which are measured at the Terra Nova Bay in the Ross Sea, are larger than those estimated here at PIG. This is consistent with the fact that katabatic wind events at Terra Nova Bay can be quite strong, being associated with much higher wind speeds than those during the Foehn events discussed here (Aulicino et al., 2018). Blowing snow sublimation (Fig. 4e) peaks just south and east of the glacier, with values in the range 0.5-0.75 mm w.e. day^{-1}, where the wind speed exceeds the threshold for blowing snow sublimation, Eq. (4). The convergence of the blowing snow transport rate from the east and southeast of PIG leads to the negative divergence at the basin (Fig. 4f). The negative values in the snowfall rate plot to the south and north of PIG, Fig. 4b, reflect the reduced precipitation in association with ~~the~~ Foehn events. The changes in the storage term between Foehn and no-Foehn timestamps, Fig. 4a, are comparable to the modelled surface mass balance in the region (Donat-Magnin et al., 2021), suggesting that Foehn events are a major contributor to it. Figs. 4g-h gives the differences in the 10-m wind speed and sensible heat flux. During Foehn episodes, there is a strengthening of the near-surface wind by 5-10 m s^{-1} with it converging into PIG. The sensible heat flux increases by about 30-40 W m^{-2}, in line with the area-averaged values in Fig. 2b. While in other regions of Antarctica, such as the Antarctica Peninsula, Foehn plays an active role in snow melting (Laffin et al., 2021), at PIG it seems to trigger mostly sublimation.

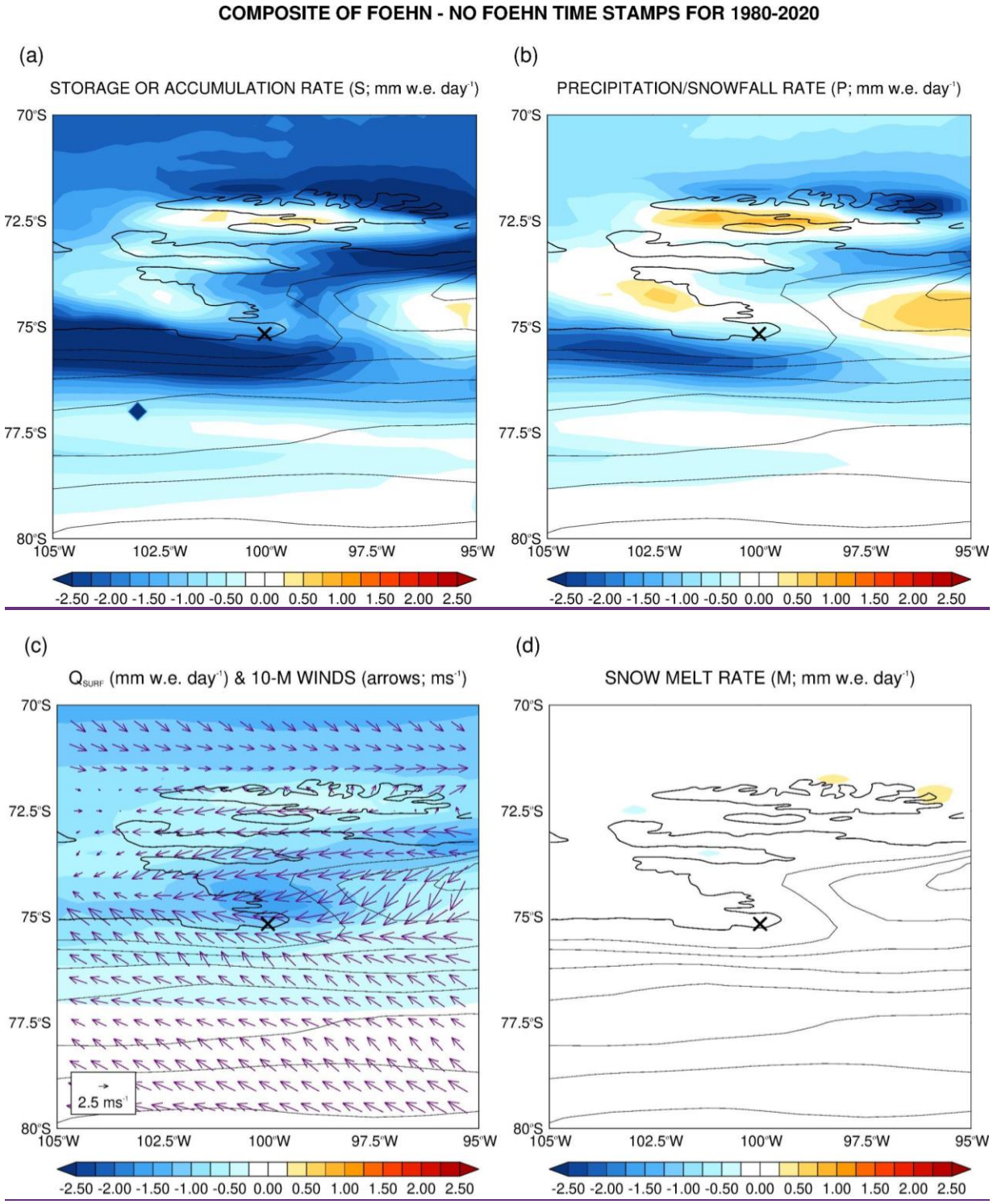
COMPOSITE OF FOEHN - NO FOEHN TIME STAMPS FOR 1980-2020
(a)
STORAGE OR ACCUMULATION RATE (S; mm w.e. day-1)
(b)
PRECIPITATION/SNOWFALL RATE (P; mm w.e. day-1)
(c)
QSURF (mm w.e. day-1) & 10-M WINDS (arrows; ms-1)
2.5 ms-1
(d)
SNOW MELT RATE (M; mm w.e. day-1)
70°S
72.5°S
75°S
77.5°S
80°S
105°W
102.5°W
100°W
97.5°W
95°W
-2.50 -2.00 -1.50 -1.00 -0.50 0.00 0.50 1.00 1.50 2.00 2.50

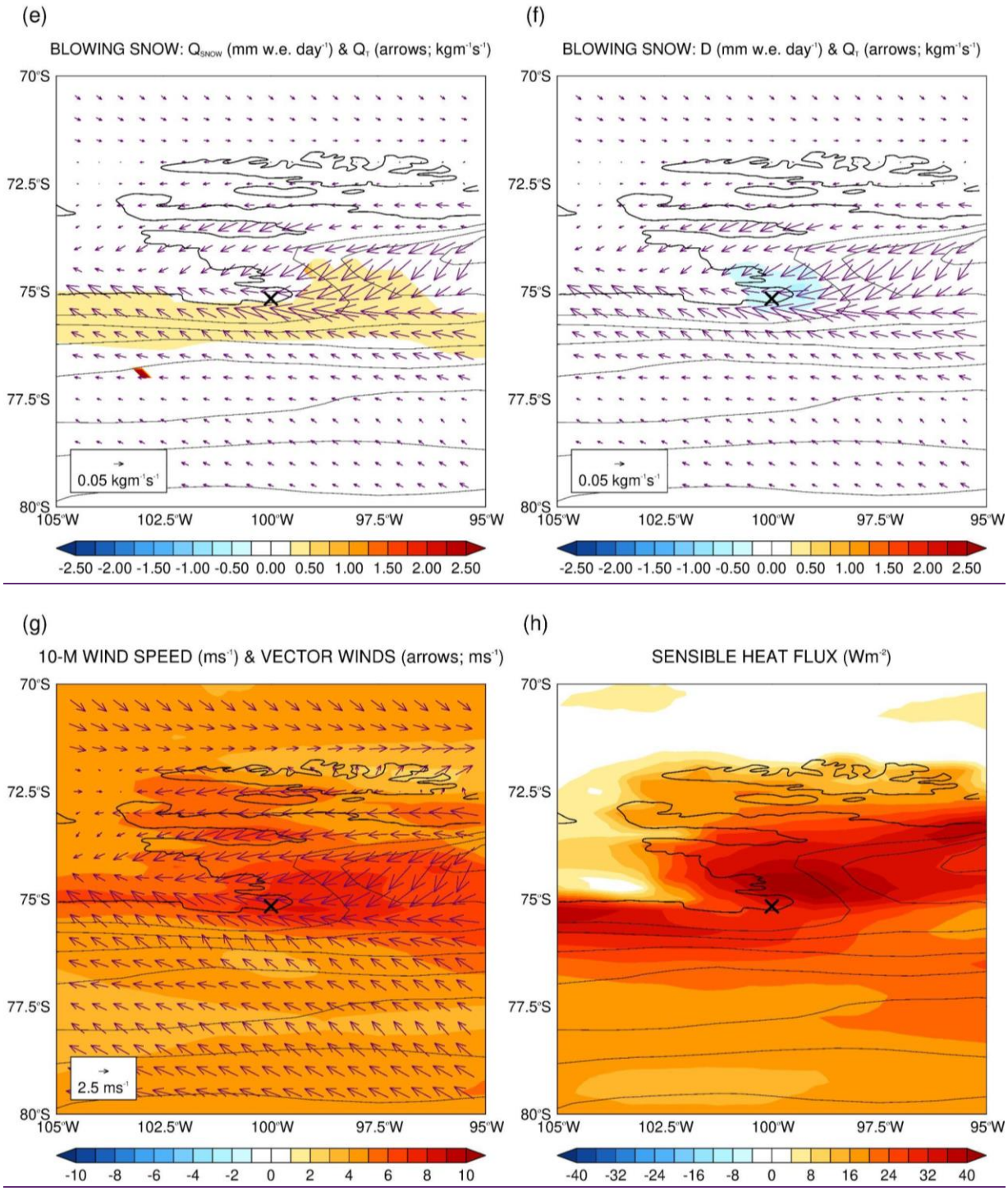

Figure 4: **Composite difference between Foehn and no-Foehn timestamps for 1980-2020:** (a) Storage or accumulation rate of snow at the surface (S in Eq. (2); mm w.e. day^{-1}), (b) precipitation/snowfall rate (P; mm w.e. day^{-1}), (c) surface sublimation rate (Q_{surf}; mm w.e. day^{-1}; positive values indicate deposition to the surface and negative values indicate sublimation), (d) snow melt rate (M; mm w.e. day^{-1}; positive values indicate melting), blowing snow (e) sublimation rate (Q_{snow}; mm w.e. day^{-1}; positive values indicate sublimation) and (f) divergence rate (D; mm w.e. day^{-1}), (g) 10-m wind speed (shading; m s^{-1}) and (h) instantaneous surface sensible heat flux (W m^{-2}, positive if downwards towards the surface). The arrows in (c) and (g) give the 10-m horizontal wind vectors (m

s^{-1}) while in (e)-(f) they show the blowing snow transport rate (Q_t; $kg\,m^{-1}s^{-1}$).

4. Large-scale Circulation Favorable for Foehn Occurrence

Foehn events are driven by large-scale pressure gradients, so it is of interest to investigate the patterns in the atmospheric circulation which promote their occurrence around PIG. The k-means clustering technique (Steinley, 2006) is applied to the daily 200 hPa and 850 hPa geopotential height and wind anomalies and to the sea-level pressure and 10-m wind anomalies for the Foehn days identified in 2000-2020. However, and to exclude localized events, only days when Foehn occurred in at least 10% of the 105º-95ºW and 70º-80ºS region are considered, leaving 1181 days for the analysis. A different number of clusters from one to five are tested, and the optimal number, as determined by a silhouette analysis (Rousseeux, 1987), is found to be two (not shown). Cluster 1 (Figs. 5a-b), which features the negative phase of the Antarctic Oscillation (AAO; Gong and Wang, 1999), accounts for ~58% of the total Foehn events. and Ccluster 2 (SAM; Figs. 5c-d), which projects onto the positive phase of the Southern Annular Mode (SAM; Marshall et al., 2003), an index which gives an indication of the strength and latitudinal position of the westerlies in the Southern Hemisphere, accounts for ~42% of the 1181 Foehn episodes. The clusters' annual cycle is given in Fig. 5e. For computational reasons the cluster analysis was not extended to 1980-2020. In any case, the findings are unlikely to change should the technique be applied to the 41-year period, with the AAO and SAM most certainly the dominant modes.

The first cluster (Fig. 5a) comprises a wavenumber #1 with an equatorward shift in the mid-latitude storm track as evidenced by the high pressure over Antarctica and a nearly circumglobal low pressure equatorwards. It corresponds to the negative phase of the AAO (Gong and Wang, 1999), with the easterly to northeasterly winds around PIG promoting the occurrence of Foehn. The air mass comes from the Weddell sector and moves over the Ellsworth Land before flowing down the length of PIG drainage basin (Fig. 5b). The wavenumber #1 is maintained by both low-latitude forcing (Quintanar and Mechoso 1995a and b) and the high topography of Antarctica (Hoskins and Karoly, 1981). As noted by Pohl et al. (2010), the AAO has a strong correlation with ENSO, with El Nino events favoring its negative phase. This mode dominates in the colder months from May to August (Fig. 5e) when the ASL is displaced westwards (Raphael et al., 2016) and hence the SAM has a smaller impact on the weather conditions at PIG.

The second cluster (Fig. 5c) projectscorresponds onto the positive phase of the SAM in which the storm track is shifted poleward and the ASL is significantly deeper (Fogt and Marshall, 2020; Zheng and Li, 2022). Mclennan and Lenaerts (2021) found that the ASL modulates the total annual snowfall at the Thwaites Glacier adjacent to PIG (Fig. 1a). This cluster shows the winds descending the slopes immediately to the east of the Pine Island ice shelf. The air mass comes from the Pacific Ocean and flows over the high terrain and coastal mountains directly to the northeast of PIG before descending downslope into the glacier basin (Fig. 5d). The cyclonic

(clockwise) circulation motion associated with the ASL, and its interaction with the high terrain to the east of PIG, leads to Foehn conditions around the glacier. Cluster #2 features a wavenumber #3 across the Southern Hemisphere.

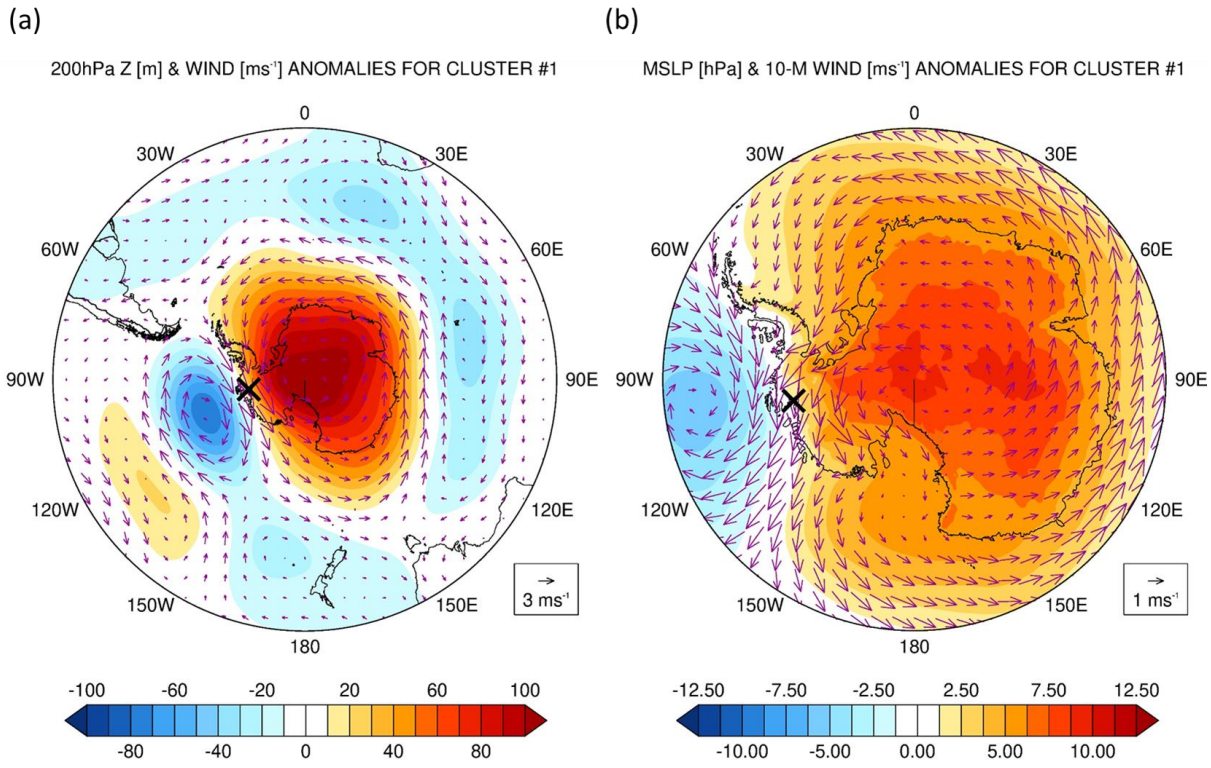

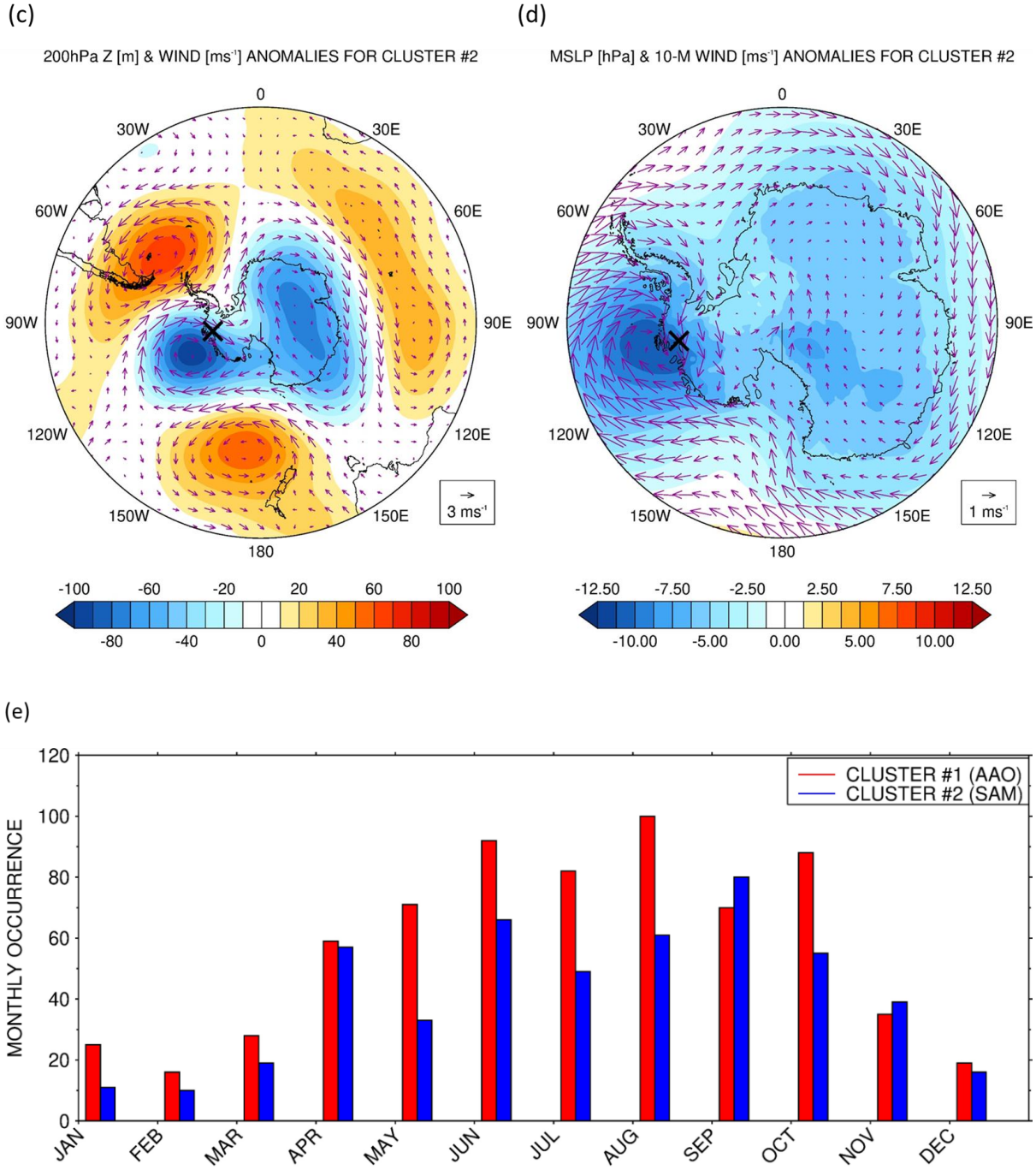

Figure 5: **Large-scale conditions promoting Foehn events:** (a) 200 hPa geopotential height anomalies (shading; m) and wind vectors (arrows; m s^{-1}) and (b) mean sea-level pressure (shading; hPa) and 10-m wind vectors (arrows; m s^{-1}) for cluster #1 of a k-means clustering technique applied to the daily-mean fields of 1181 Foehn days at PIG in 2000-2020. The cross gives the approximate location of PIG (100ºW, 75º10'S). (c)-(d) are as (a)-(b) but for cluster #2. The monthly occurrence of each cluster is given in panel (e).

5. Illustrative Case Study: November 2011

The effects of Foehn at PIG are discussed for an event in November 2011. Fig. 6 summarises the large-scale environment that promoted the occurrence of Foehn, while Fig. 7 presents a time-series of spatially-averaged meteorological variables that allows for a quantification of the Foehn effects.

The ASL was particularly deep on 10-11 November 2011, with the 500 hPa geopotential height anomalies more than 1.5 ∫ below the 1979-2020 mean (Figs. 6a-b). An atmospheric river associated with an elongated and narrow band of high moisture content and integrated vapour transport (IVT) values in the top 10% of the climatological distribution, extended from the Southern Hemisphere mid-latitudes into West Antarctica and PIG, being transported by the clockwise circulation of the ASL. As the ASL edged closer to the Antarctica Peninsula on 11 November (Fig. 6b), the more moist air, now over the Weddell Sea, penetrated further inland reaching PIG and the surrounding region from the east (after flowing over the ice divide that separates the Weddell Sea and Ronne Ice Shelf from PIG and the Amundsen Sea region). As a result, the IVT at PIG more than doubled from about 27.5 $kg\,m^{-1}\,s^{-1}$ on 10 November to around 65 $kg\,m^{-1}\,s^{-1}$ on 11 November, with the total column water vapour increasing to just under 4 $kg\,m^{-2}$ (Fig. 7a). The Foehn effect in this event corresponds to that of cluster #1 (Fig. 4a), the more indirect pathway from the Weddell Sea as opposed to Foehn events triggered by Pacific warm air intrusions (cluster #2, Fig. 4b).

As seen in Figs. 6c-d, the air mass accelerated downslope as it descended the mountains towards coastal West Antarctica, with 10-m wind speeds higher than 20 $m\,s^{-1}$ and in the top 10% of the climatological distribution over a vast region including PIG (locally in the top 1% just to the northwest and southeast of PIG), and downward sensible heat fluxes in excess of 75 $W\,m^{-2}$ at PIG (the negative, or upward pointing, fluxes around 75ºS and 110ºW are associated with a sea ice-free area). These tendencies are seen in the area-averaged time-series (Fig. 7c) with the negative (upward) latent heat flux indicating sublimation peaking on 11 November (Fig. 7f). In fact, the phase of the latent heat flux matches that of the surface sublimation given in Fig. 7f. The opposite sign of the sensible and latent heat fluxes, which roughly offset each other, is expected during Foehn events (Elvidge et al., 2020), as the positive latent heat flux which arises due to sublimation is opposed by the downward sensible heat flux due to the higher air than surface temperature. The surface mass balance is essentially controlled by the surface and blowing snow sublimation, with the precipitation/snowfall and the divergence terms playing a secondary role, and with the snow melting being zero throughout the full period (Fig. 7f). The estimated maximum sublimation rate is seen at the end of 10 November and has a magnitude of ~0.13 mm w.e. hr^{-1}, comparable to the ice loss due to ocean dynamics (e.g., Holland et al., 2007; Rintoul et al., 2016; Feldmann et al., 2019) albeit in a non-sustained way. The ERA-5 snow depth, which accounts only for sublimation and changes in snow density (snow melt is not simulated by ERA-5 during this event, Fig. 7f), shows a steady decrease starting on 04 November and a faster drop from 11-13 November (not

shown). The reanalysis snow depth during this period is around 9.21 m w.e., within the range of that observed during field campaigns discussed in Konrad et al. (2019). Besides sublimation, melting was detected in the Moderate Resolution Imaging Spectroradiometer (MODIS; Kaufman et al., 1997) satellite imagery reaching a maximum on 12 November (Fig. 7g). The melting area at times exceeded ~100 km^2 or roughly 2% of the central trunk of the glacier (Wingham et al., 2009). The fact that ERA-5 does not simulate the observed melting can be attributed to the way snow melting is parameterized in the model used to generate the reanalysis dataset, only taking place if the temperature of the snow layer exceeds the melting point (ECMWF, 2016), with ERA-5 exhibiting a cold bias over the high terrain in Antarctica (e.g. Gonzalez et al., 2021). The observed melting area is also much smaller than ERA-5's spatial resolution (~27 km × 27 km). Further insight into the surface melt can be gained by running a surface balance model at high spatial resolution that can be driven by ERA-5 data. This will be left for future work.

In Figs. 7d-e, the net shortwave, longwave and radiation fluxes from the reanalysis data are compared with those estimated from satellite data, as given by the Clouds and Earth's Radiant Energy System (CERES) SYN1deg dataset (Doelling et al. 2013, 2016). ERA-5 under-predicts the net shortwave radiation flux during the day by up to a factor of 2.5, and the net longwave radiation flux at night by up to 25 $W m^{-2}$. These differences are consistent with those reported by Ghiz et al. (2021), who attributed the lower shortwave fluxes in ERA-5 compared to CERES to differences in the cloud properties, with the reanalysis fluxes being more consistent with those measured in situ at a site in the West Antarctic Ice Sheet than those of CERES. On the other hand, CERES partially corrects the tendency of ERA-5 to under-predict the net longwave radiation flux over Antarctica, in particular in clear-sky conditions (Silbert et al., 2019). During the November Foehn event, the area-averaged surface energy flux, F_{net}, is positive (Fig. 7e), as the positive sensible heat flux offsets the negative latent heat flux (Fig. 7c), and the surface net shortwave radiation flux overwhelms the negative net longwave flux (Fig. 7d). This indicates an excess of energy towards the surface leading to snow melt and evaporation. The 3-5ºC increase in air temperature (Fig. 7b) with respect to the previous non-Foehn days, present both in the reanalysis and weather station data, is comparable to that seen during a Foehn event at the Ross Ice Shelf in January 2016 (Zou et al., 2019). Note that the ERA-5 values are area-averaged over the red box in Fig. 1a and hence the fields are likely larger in local areas.

The Foehn event can also be seen in the Hovmoeller plots in Fig. 6e. The wind direction shifts from northeast to southeast on 08-09 November 2011 around PIG as the ASL moves closer to the Antarctica Peninsula. This is accompanied by an increase in the sensible heat flux, with a latitudinally-averaged value exceeding 50 $W m^{-2}$ that corresponds to an anomaly of about 40 $W m^{-2}$. The fact that the peak in wind speed takes place ~90ºW but that in the heat fluxes around 100º-110ºW is consistent with the warming of the air mass as it descends the slopes of the mountains over West Antarctica. The drying of the atmosphere in association with the Foehn effects is also present, with the RH dropping below 70% during the event. The sensible heat flux shows a clear

diurnal cycle, peaking around 05-06 UTC, which is roughly 00 Local Time (LT) for a longitude of ~100ºW, out-of-phase with the surface radiation fluxes (Figs. 7c-e). This mismatch is also seen on other days, and may be attributed to the effects of Foehn, clouds and moisture on the heat fluxes. Weaker Foehn events, with peak wind speeds roughly half of that on 09-11 November but similar values of RH, took place earlier in the month, on 03-04 November 2011.

(a)

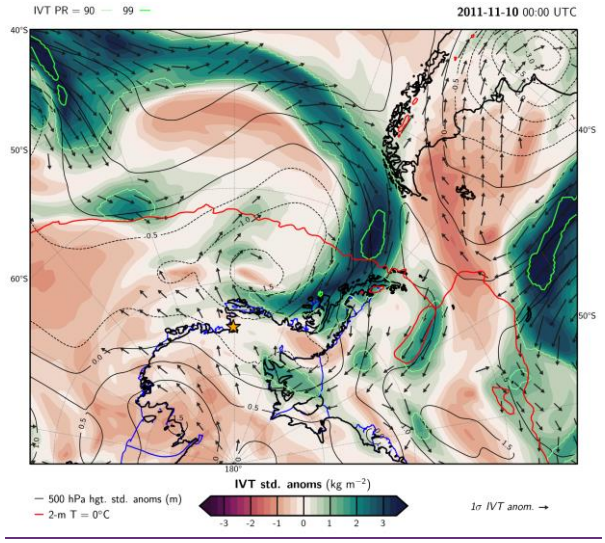

(b)

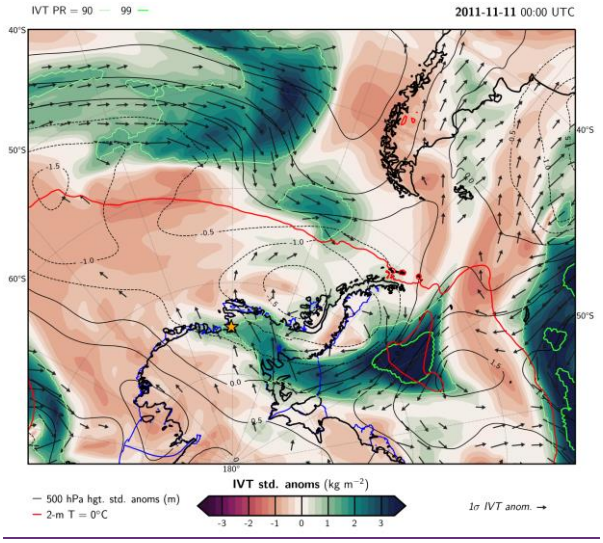

(c)

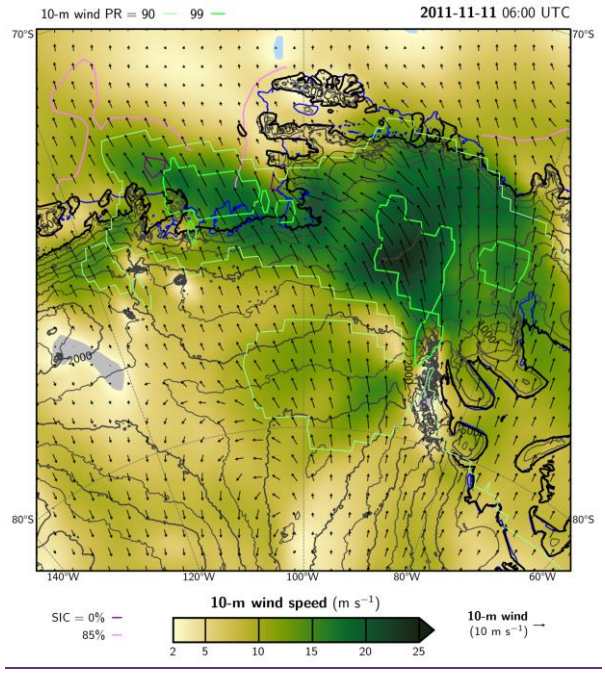

(d)

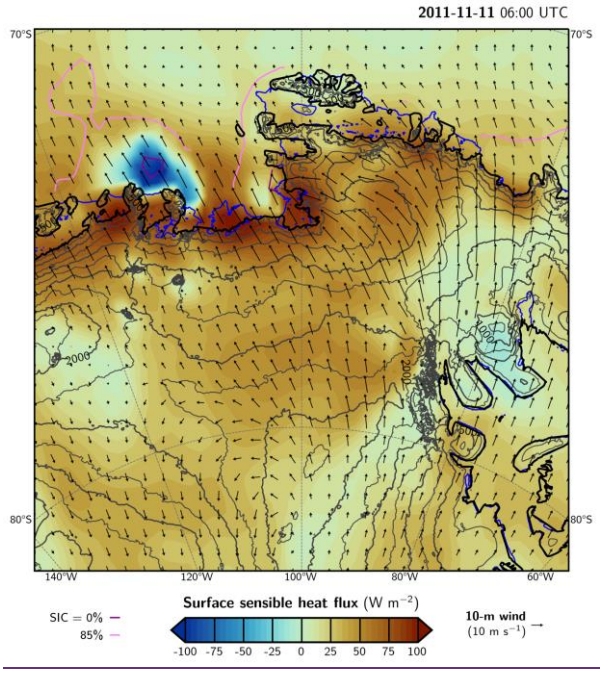

(e)

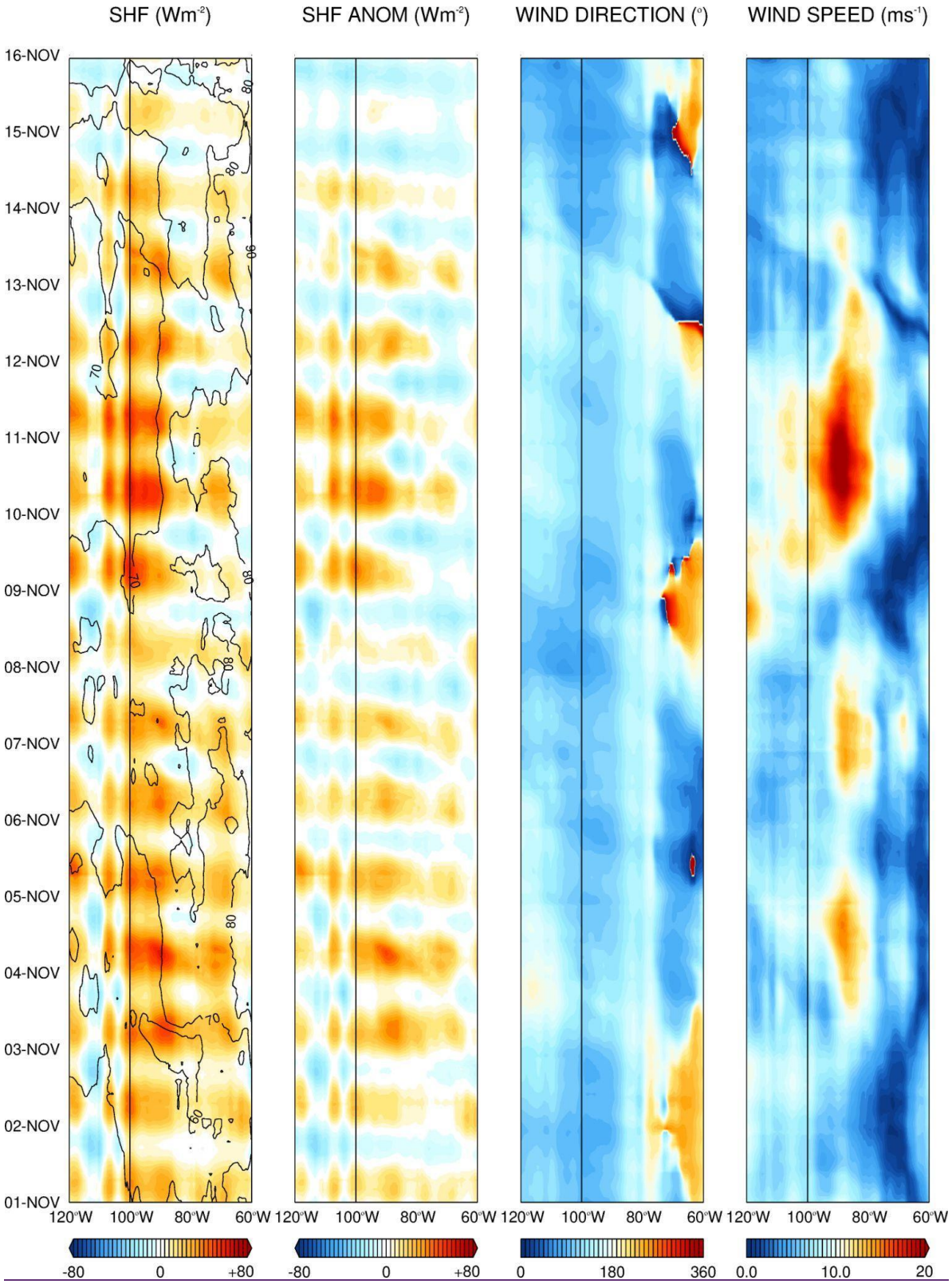
SHF (Wm-2)
SHF ANOM (Wm-2)
WIND DIRECTION (°)
WIND SPEED (ms-1)
16-NOV
15-NOV
14-NOV
13-NOV
12-NOV
11-NOV
10-NOV
09-NOV
08-NOV
07-NOV
06-NOV
05-NOV
04-NOV
03-NOV
02-NOV
01-NOV
120°W 100°W 80°W 60°W
-80 0 +80
0 180 360
0.0 10.0 20

Figure 6: **November 2011 Foehn events:** Integrated Water Vapour Transport (IVT; kg m^{-2}; shading) standardized ~~normalised~~ anomalies with respect to ERA-5's 1979-2020 monthly climatology, the vectors give a one standard deviation anomaly and are only~~is~~ plotted if the IVT standardized anomalies exceed one~~as vectors~~, and 500 hPa geopotential height standardized anomalies (solid~~m;~~ contours) on (a) 10 November and (b) 11 November 2011 at 00 UTC. The thin and thick green lines denote the 90th and 99th IVT percentiles, respectively, the yellow star gives the location of the Evans Knoll weather station (-74.85ºS; -100.404ºW), and the red solid line is the 0ºC 2-m temperature isotherm. (c) 10-m wind speed (shading; m s^{-1}), with the 90th and 99th percentiles denoted by the solid thin and thick green lines, respectively, ~~mean sea level pressure (solid black contours; hPa)~~ and 10-m winds (vectors; m s^{-1}) on 11 November 2011 at 06 UTC. The grey lines are orographic contours drawn and labelled every 500 m, and the dark solid purple and pink lines highlight regions where the sea-ice concentration is equal to 0% and 85%, respectively. (d) is as (c) but with the shading giving the sensible heat flux (shading; W m^{-2}), positive if downwards towards the surface. ~~In panels (a)-(d), the red solid~~dashed line is the 0ºC 2-m temperature isotherm, and ~~the dark solid purple and pink lines highlight regions where the sea-ice concentration is equal to 0% and 85%, respectively.~~ The anomalies and percentile ranks for the IVT, 10-m horizontal winds, 500 hPa geopotential height and 2-m temperature are calculated from the distribution of all 3-h values within +/- 15 Julian days from the given date during the 1979–2020 period and at a given grid point. (e) Hovmoeller plot of sensible heat flux (shading; W m^{-2}) and relative humidity (contours, every 10%), sensible heat flux anomalies with respect to the 1979-2021 climatology (W m^{-2}), and 10-m wind direction (º) and speed (m s^{-1}) for 01-15 November 2011. The fields are averaged over 72.5º-77.5ºS and are plotted for the region 120ºW-60ºW. All colour bars are linear with only the lowest, middle and highest values shown. The black vertical line indicates the approximate longitude of PIG (100ºW).

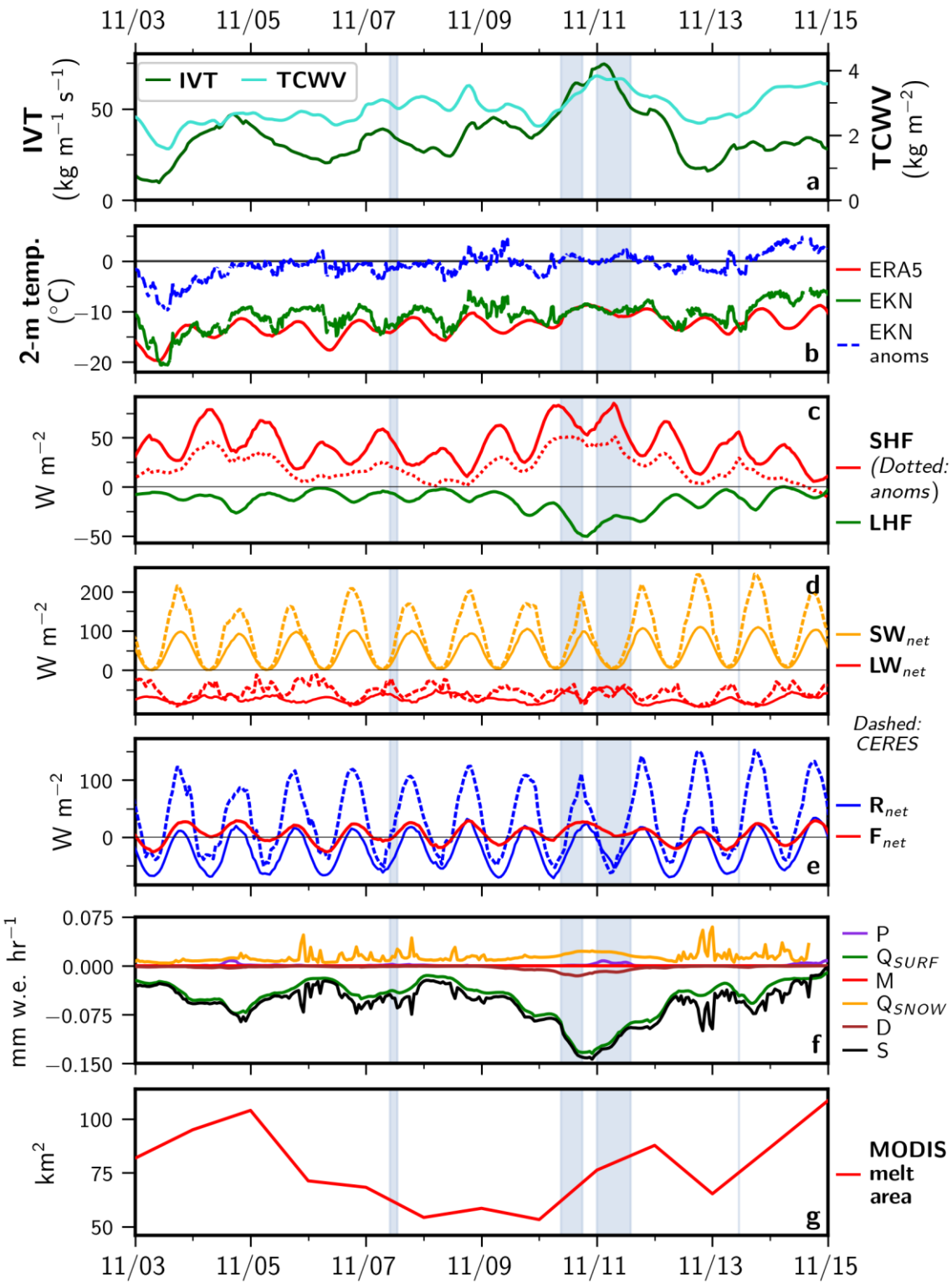

Figure 7: **Impacts of Foehn winds on ice:** Time series of 1-hourly ERA-5 variables averaged over PIG (red box in Fig. 1a) from 03 to 14 November 2011: (a) Integrated water vapor transport (IVT; light green; kg m^{-1} s^{-1}) and total column water vapor (TCWV; dark green; kg m^{-2}); (b) 10-min observed 2-m temperature (green; ºC) at the Evans Knoll weather station (-74.85ºS, -100.404ºW; 188 m above sea-level), the anomalies with respect to the 2011-2015

hourly climatology are given by the dashed blue line, and area-averaged ERA-5 2-m temperature (red; ºC); (c) ERA-5 sensible heat flux (SHF; red; W m^{-2}) and latent heat flux (LHF; orange; W m^{-2}); (d) net shortwave radiation (SW_{net}; orange; W m^{-2}) and longwave radiation (LW_{net}; red; W m^{-2}) flux at the surface; (e) net radiation (R_{net}; blue; W m^{-2}) and total energy flux ($F_{net} = SHF + LHF + R_{net}$; red; W m^{-2}) at the surface; (f) individual components of the surface mass balance, Eq. (2), expressed in mm w.e. hr^{-1}. The S, P, M, Q_{surf}, Q_{snow} and D terms are given by the black, purple, red, green, orange and brown lines, respectively; (g) Daily total surface area (km^2) of melt ponds observed from MODIS imagery. In panel (c), the SHF anomalies, calculated as the difference from the domain-averaged 1979-2020 November hourly monthly mean, are also plotted. In (d)-(e), the net radiative variables from CERES averaged over the same domain are plotted as dashed lines for comparison. Times when Foehn occurred are shaded in blue.

6. Discussion and Conclusions

Pine Island Glacier (PIG), located in West Antarctica around 75ºS and 100ºW between the Antarctic Peninsula to the east and the Ross Ice Shelf to the west, has been losing ice mass at an accelerated rate over the last two decades. While the vast majority of the studies on ice loss at PIG focus on ocean dynamics (e.g. Stanton et al., 2013; Favier et al., 2014), atmospheric forcing is also likely to be important, with warmer and more moist air intrusions from the mid-latitudes and Foehn effects the likely candidates (Ghiz et al., 2021). The role of moist air intrusions is well documented (e.g. Willie et al., 2021), but less attention has been paid to Foehn, in particular around PIG where the complex terrain promotes its occurrence. Foehn effects can lead to ice loss through sublimation, which is typically a small-scale and invisible phenomenon in nature and hence difficult to be detected using satellite data. At the same time, Foehn plays an important role in the surface mass balance around Antarctica (Ghiz et al., 2021), and a better understanding of its occurrence may help to reduce the major uncertainties that still exist (The IMBIE team, 2018). In this work, a 41-year climatology of Foehn events at PIG is generated using ERA-5 reanalysis data, and its impact on the surface mass balance is analyzed. The large-scale atmospheric circulation patterns that favor Foehn events at PIG are also identified.

Foehn events at PIG are more frequent in the colder months from June to October, with an average of 3.0 events per month in the 105º-95ºW and 70º-80ºS region in August 1980-2020 and just 0.37 in January. The peak in austral winter is consistent with the poleward position of the mid-latitude storm track, with the Amundsen Sea Low (ASL), a semi-permanent low pressure in the Amundsen-Bellingshausen Seas, closest to the Antarctica coast in late winter. The presence of a low just north of PIG favours easterly to southeasterly winds at the site, which encourages the occurrence of Foehn. The duration of Foehn events exhibits a less pronounced annual cycle, with Foehn episodes typically lasting 5 to 9 h. ~~Both the number and duration of Foehn events at PIG are smaller than those at other sites around Antarctica such as the Antarctic Peninsula, due to the reduced exposure to the mid-latitude baroclinic systems.~~

The negative phase of the Antarctic Oscillation, in particular in the cold season (May to August), and the positive phase of the Southern Annular Mode, foster the occurrence of Foehn at PIG. The former is a more indirect pathway, with the air flow coming from the Weddell sector and moving

over the Ellsworth Land before reaching PIG, while in the latter the air mass comes from the Pacific Ocean and flows over the high terrain directly to the northeast of PIG before descending into the glacier basin. ~~A trend analysis revealed that Foehn events have been occurring more frequently (at a rate of about 4.1 days/41 years) in 1980-2020. There is, however, considerable inter-annual variability, with the peaks generally coinciding with La Nina or neutral episodes, while the lower values in El Nino events are associated with a weaker ASL.~~

A composite of Foehn and no-Foehn episodes revealed that Foehn events have an important impact on the surface mass balance. It is concluded that surface sublimation plays the major role, with a magnitude of ~1.434 mm water equivalent (w.e.) day^{-1}, comparable to that observed at other sites in Antarctica. The blowing snow sublimation and divergence rate have a comparable magnitude to that of the precipitation (snowfall) rate, with values of 0.35-0.36 mm w.e. day^{-1}. However, while the former makes a positive contribution to the surface mass balance due to the convergence of the snow transport rate at the glacier basin, the latter depletes surface snow, as the drier conditions associated with Foehn reduce the likelihood of the occurrence of precipitation. The melting rate is negligible and is restricted to the coastal areas to the north of the glacier.

A particularly strong Foehn event took place on 09-11 November 2011. During this period the ASL was more than 1.5 standard deviations stronger than the 1979-2020 climatological mean, with an atmospheric river from the Southeast Pacific injecting moisture into West Antarctica through the Weddell Sea. As the southeasterly winds descended the high terrain east and southeast of the glacier they accelerated, with 10-m wind speeds in excess of 20 m s^{-1} and in the top 10% of the climatological distribution, and downward sensible heat fluxes higher than 75 W m^{-2}, a clear signature of Foehn effects. Besides surface sublimation, at a rate of up to 0.13 mm w.e. hr^{-1}, melting was detected using satellite data with the hourly melting area at times in excess of 100 km^2.

As Foehn has been shown to play an important role in modulating ice conditions elsewhere around Antarctica such as in the Antarctic Peninsula (Massom et al., 2018) and Ross Ice Shelf (Zou et al. 2021a and b), a detailed analysis of Antarctica-wide Foehn occurrence is needed to better quantify its contribution to snow sublimation and ice loss. The fact that Foehn winds are more effective in inducing snow sublimation than snow melt at PIG, makes it challenging to detect their total impact on the ice state at the scale of the continent as snow evaporation cannot be detected from space. Advanced remote sensing techniques to detect changes in the depth of the snow layer over land ice are therefore needed.

Acknowledgment

The authors wish to acknowledge the contribution of Khalifa University's high-performance computing and research computing facilities to the results of this research. This work has been supported by Masdar Abu Dhabi Future Energy Company through research grant number

8434000222. We also appreciate the support of the University of Wisconsin-Madison Automatic Weather Station Program for the data set and information, NSF grant number 1924730. We would like to thank the two anonymous reviewers for their insightful and constructive comments and suggestions that have substantially improved the quality of this manuscript.

Code Availability

The scripts used to process MODIS data and estimate the melting area are available upon request from Dr. Catherine Walker (catherine.c.walker@nasa.gov). The codes used to estimate the terms in the surface mass balance can be requested from Prof. Diana Francis (diana.francis@ku.ac.ae).

Data Availability

All the data used to generate the figures in this study has been uploaded to Francis et al. (2023). ERA-5 hourly reanalysis surface (Hersbach et al. 2018b) and pressure-level (Hersbach et al. 2018a) data used in this work is freely available online on Copernicus' Climate Change Service Climate Data Store website. The weather data for the Evans Knoll station located next to Pine Island Glacier (PIG) is freely available at the Antarctic Meteorological Research Center & Automatic Weather Stations Project website (Lazzara et al., 2022). The Antarctic 1 km Digital Elevation Model (DEM) from Combined ERS-1 Radar and ICESat Laser Satellite Altimetry, Version 1 (NSIDC-0422; Bamber et al. 2009a) used to plot Antarctica surface elevation, MEaSUREs InSAR-Based Antarctica Ice Velocity Map, Version 2 (NSIDC-0484; Rignot et al. 2017) used to plot mean ice velocity of Pine Island and Thwaites Glaciers, and MEaSUREs Antarctic Boundaries for IPY 2007-2009 from Satellite Radar, Version 2 (NSIDC-0709; Mouginot et al. 2017) are freely available available from the National Aeronautics and Space Administration National Snow and Ice Data Center (NSIDC) Distributed Active Archive Center website. The Clouds and Earth's Radiant Energy System (CERES) surface fluxes product SYN1deg - Level 3 has been made publicly available at NASA/LARC/SD/ASDC (2017). Sentinel-2 satellite data, used to extract the sea-ice front at PIG, is available online at (Copernicus, 2022). The MODIS daily global surface reflectance Level 3 data (MOD09CMG, MYD09CMG; Vermote 2015a,b) are publicly available from NASA Earthdata. The figures presented in this paper were generated using the Interactive Data Language (IDL; Bowman, 2005) software version 8.8.1 and the Matplotlib (Hunter, 2007) and Cartopy (Met Office, 2014) python libraries.

Author Contribution

DF conceived the study. RF and DF wrote the manuscript with inputs from KSM, SL and CW. SL and CW processed the MODIS data while RF and KSM analyzed the reanalysis data. DF provided formal analysis and validation of the results.

Conflict of Interest

SL is a member of the editorial board of The Cryosphere and this is handled according to the journal policies.

References

Adusumilli, S., Fish, M. A., Fricker, H. and Medley, B. (2021) Atmospheric river precipitation contributed to rapid increases in surface height of the West Antarctic Ice Sheet in 2019. Geophysical Research Letters, 48, e2020GL091076. https://doi.org/10.1029/2020GL091076.

Aulicino, G., Sansiviero, M., Paul, S., Cesarano, C., Fusco, G., Wadhams, P., Budillon, G. (2018) A New Approach for Monitoring the Terra Nova Bay Polynya through MODIS Ice Surface Temperature Imagery and Its Validation during 2011 and 2011 Winter Seasons. Remote Sensing, 10, 366. https://doi.org/10.3390/rs10030366.

[Dataset] Bamber, J., Gomez-Dans, J. L. and Griggs, J. A. (2009a) Antarctic 1km Digital Elevation Model (DEM) from Combined ERS-1 Radar and ICESat Laser Satellite Altimetry, version 1. Boulder, Colorado USA. National Aeronautics and Space Administration National Snow and Ice Data Center Distributed Active Archive Center. Accessed on 26 April 2022, available online at https://doi.org/10.5067/H0FQ1KL9NEKM.

Bamber, J. L., Riva, R. E. M., Vermeersen, B. L. A. and LeBrocq, A. M. (2009b) Reassessment of the potential sea-level rise from a collapse of the West Antarctic Ice Sheet. Science, 324, 901-903. https://doi.org/10.1126/science.1169335.

Bell, R. E., Banwell, A. F., Trusel, L. D. and Kingslake, J. (2018) Antarctic surface hydrology and impacts on ice-sheet mass balance. Nature Climate Change, 8, 1044-1052. https://doi.org/10.1038/s41558-018-0326-3.

Bowman, K. P. (2005) An Introduction to Programming with IDL: Interactive Data Language [Software]. Academic Press, 304 pp., ISBN-10: 012088559X, ISBN-13: 978-0120885596.

Bozkurt, D., Rondanelli, R., Marin, J. C. and Garreaud, R. (2018) Foehn event triggered by an atmospheric river underlies record-setting temperature along continental Antarctica. Journal of Geophysical Research: Atmospheres, 123, 3871-3892. https://doi.org/10.1002/2017JD027796.

Bromwich, D. H. (1989) Satellite Analysis of Antarctic Katabatic Wind Behavior. Bulletin of the American Meteorological Society, 70, 738-749. https://doi.org/10.1175/1520-0477(1989)070<0738:SAOAKW>2.0.CO;2.

~~Cape, M. R., Vernet, M., Kahru, M. and Spreen, G. (2014) Polynya dynamics drive primary production in the Larsen A and B embayments following ice shelf collapse. Journal of Geophysical Research: Oceans, 119, 572-594. https://doi.org/10.1002/2013JC009441.~~

~~Cape, M. R., Vernet, M., Skvarca, P., Marinsek, S., Scambos, T. and Domack, E. (2015) Foehn winds link climate-driven warming to ice shelf evolution in Antarctica. Journal of Geophysical Research: Atmospheres, 120, 11037-11057. https://doi.org/10.1002/2015JD023465.~~

[Dataset] Copernicus (2022) Copernicus Open Access Hub. Available online at https://scihub.copernicus.eu/, accessed on 10 October 2022.

Das, I., Bell, R. E., Scambos, T. A., Wolovick, M., Creyts, T. T., Studinger, M., Frearson, N., Nicolas, P., Lenaerts, J. T. M. and van den Broeke, M. (2013) Influence of persistent wind scour on the surface mass balance of Antarctica. Nature Geoscience, 6, 367-371. https://doi.org/10.1038/ngeo1766.

Datta, R. T., Tedesco, M., Fettweis, X., Agosta, C., Lhermitte, S., Lenaerts, J. T. M., Wever, N. (2019) The effect of Foehn-induced surface melt on firn evolution over the northeast Antarctic peninsula. Geophysical Research Letters, 46, 3822-3831. https://doi.org/10.1029/2018GL080845.

De Rydt, J., Reese, R., Paolo, F. S. and Gudmundsson, G. H. (2021) Drivers of Pine Island Glacier speed-up between 1996 and 2016. The Cryosphere, 15, 113-132. https://doi.org/10.5194/tc-15-113-2021.

Dery, S. J., Yau, M. K. (1999) A Bulk Blowing Snow Model. Boundary-Layer Meteorology, 93, 237-251. https://doi.org/10.1023/A:1002065615856.

Dery, S. J., Yau, M. K. (2002) Large-scale mass balance effects of blowing snow and surface sublimation. Journal of Geophysical Research, 107, 4679. https://doi.org/10.1029/2001JD001251.

Dias da Silva, P. E., Hodges, K. I., Coutinho, M. M. (2021) How well does the HadGEM2-ES coupled model represent the Southern Hemisphere storm tracks? Climate Dynamics, 56, 1145-1162. https://doi.org/10.1007/s00382-020-05523-9.

Dirscherl, M. C., Dietz, A. J., Kuenzer, C. (2021) Seasonal evolution of Antarctic supraglacial lakes in 2015-2021 and links to environmental controls. The Cryosphere, 15, 5205-5226. https://doi.org/10.5194/tc-15-5205-2021.

Djoumna, G. and Holland, D. M. (2021) Atmospheric rivers, warm air intrusions, and surface radiation balance in the Amundsen Sea Embayment. Journal of Geophysical Research: Atmospheres, 126, e2020JD034119. https://doi.org/10.1029/2020JD034119.

Doelling, D. R., Loeb, N. G., Keyes, D. F., Nordeen, M. L., Morstad, D., Nguyen, C., Wielicki, B. A., Young, D. F. and Sun, M. (2013) Geostationary Enhanced Temporal Interpolation for CERES Flux Products. Journal of Atmospheric and Oceanic Technology, 30, 1072-1090. https://doi.org/10.1175/JTECH-D-12-00136.1.

Doelling, D. R., Sun, M., Nguyen, L. T., Nordeen, M. L., Haney, C. O., Keyes, D. F. and Mlynczak, P. E. (2016) Advances in Geostationary-Derived Longwave Fluxes for the CERES Synoptic (SYN1deg) Product.

Journal of Atmospheric and Oceanic Technology, 33(3), 503-521. https://doi.org/10.1175/JTECH-D-15-0147.1.

Donat-Magnin, M., Jourdain, N. C., Kittel, C., Agosta, C., Amory, C., Gallee, H, Kinner, G., Chekki, M. (2021) Future surface mass balance and surface melt in the Amundsen sector of the West Antarctic Ice Sheet. The Cryosphere, 15, 571-593. https://doi.org/10.5194/tc-15-571-2021.

ECMWF (2016) IF Documentation - Cy43r1 Operational Implementation 22 Nov 2016. Part IV: Physical Processes. Accessed on 26 October 2022, available online at https://www.ecmwf.int/sites/default/files/elibrary/2016/17117-part-iv-physical-processes.pdf.

Elvidge, A. D., Kuipers Munneke, P., King, J. C., Renfrew, I. A., Gilbert, E. (2020) Atmospheric drivers of melt on Larsen C Ice Shelf: Surface energy budget regimes and the impact of foehn. Journal of Geophysical Research: Atmospheres, 125, e2020JD032463. https://doi.org/10.1029/2020JD032463.

Elvidge, A. D. and Renfrew, I. A. (2016) The Causes of Foehn Warming in the Lee of Mountains. Bulletin of the American Meteorological Society, 97(3), 455-466. https://doi.org/10.1175/BAMS-D-14-00194.1.

Elvidge, A. D., Renfrew, I. A., King, J. C., Orr, A., Lachlan-Cope, T. A. (2016) Foehn warming distributions in nonlinear and linear flow regimes: a focus on the Antarctic Peninsula. Quarterly Journal of the Royal Meteorological Society, 142, 618-631. https://doi.org/10.1002/qj.2489.

Favier, L., Durand, G., Cornford, S. L., Gudmundsson, G. H., Gagliardini, O., Gillet-Chaulet, F., Zwinger, T., Payne, A. J. and Le Brocq, A. M. (2014) Retreat of Pine Island Glacier controlled by marine ice-sheet instability. Nature Climate Change, 4, 117-121. https://doi.org/10.1038/nclimate2094.

Feldmann, J., Levermann, A., Mengel, M. (2019) Stabilizing the West Antarctic Ice Sheet by surface mass deposition. Science Advances, 5. https://doi.org/10.1126/sciadv.aaw4132.

Fogt, R. L. and Marshall, G. J. (2020) The Southern Annular Mode: Variability, trends, and climate impacts across the Southern Hemisphere. WIREs Climate Change, 11, e625. https://doi.org/10.1002/wcc.652.

Francis, D., Fonseca, R., Mattingly, K., Lhermitte, S. and Walker, C. (2023) Datasets for the publication "Foehn Winds at Pine Island Glacier and its role in Ice Shelf Sublimation and Surface Melt" [Dataset]. Zenodo, https://zenodo.org/record/7707591.

Francis, D., Fonseca, R., Mattingly, K. S., Marsh, O. J., Lhermitte, S. and Cherif, C. (2022) Atmospheric triggers of the Brunt Ice Shelf calving in February 2021. Journal of Geophysical Research: Atmospheres, 127, e2021JD036424. https://doi.org/10.1029/2021JD036424.

Francis, D., Mattingly, K. S., Lhermitte, S., Temimi, M. and Heil, P. (2021) Atmospheric extremes caused high oceanward sea surface slope triggering the biggest calving event in more than 50 years at the Amery Ice Shelf. The Cryosphere, 15, 2147-2165. https://doi.og/10.5194/tc-15-2147-2021.

Francis, D., Mattingly, K. S., Temimi, M., Massom, R. and Heil, P. (2020) On the crucial role of atmospheric rivers in the two major Weddell Polynya events in 1973 and 2017 Antarctica. Science Advances, 6, eabc2695. https://doi.org/10.1126/sciadv.abc2695.

Gehring, J., Vignon, E., Billaut-Roux, A.-C., Ferrone, A., Protat, A., Alexander, S. P., Berne, A. (2022) Orographic flow influence on precipitation during an atmospheric river event at Davis, Antarctica. Journal of Geophysical Research: Atmospheres, 127, e2021JD035210. https://doi.org/10.1029/2021JD035210.

Ghiz, M. K., Scott, R. C., Vogelmann, A. M., Lenaerts, J. T. M., Lazzara, M. and Lubin, D. (2021) Energetic of surface melt in West Antarctica. The Cryosphere, 15, 3459-3494. https://doi.org/10.5194/tc-15-3459-2021.

Gong, D. and Wang, S. (1999) Definition of Antarctic oscillation index. Geophysical Research Letters, 26(4), 459-462. https://doi.org/10.1029/1999GL900003.

Gonzalez, S., Vasallo, F., Sanz, P., Quesada, A. and Justel, A. (2021) Characterization of the summer surface mesoscale dynamics at Dome F, Antarctica. Atmospheric Research, 259, 105699. https://doi.org/10.10.1016/j.atmosres.2021.105699.

~~Gorodetskaya, I. V., Kneifel, S., Maahn, M., Van Tricht, K., Thiery, W., Schween, J. H., Mangold, A., Crewell, S., Van Lipzig, N. P. M. (2015) Cloud and precipitation properties from ground-based remote-sensing instruments in East Antarctica. The Cryosphere, 9, 285-304. https://doi.org/10.5194/tc-9-285-2015.~~

Gossart, A., Helsen, S., Lenaerts, J. T. M., Vanden Broucke, S., van Lipzig, N. P. M. and Souverijns, N. (2019) An Evaluation of Surface Climatology in State-of-the-Art Reanalyses over the Antarctic Ice Sheet. Journal of Climate, 32(20), 6899-6915. https://doi.org/10.1175/JCLI-D-19-0030.1.

Goyal, R., Jucker, M., Gupta, A. S., Hendon, H. H. and England, M. H. (2021) Zonal wave 3 pattern in the Southern Hemisphere generated by tropical convection. Nature Geosciences, 14, 732-738. https://doi.org/10.1038/s41561-021-00811-3.

Greene, C. A., Gardner, A. S., Schlegel, N.-J. and Fraser, A. D. (2022) Antarctic calving loss rivals ice-shelf thinning. Nature, 609, 948-953. https://doi.org/10.1038/s41586-022-050307-w.

[Dataset] Hersbach, H., Bell, B., Berrisford, P., Biavati, G., Horanyi, A., Munoz Sabater, J., Nicolas, J., Peubey, C., Radu, R., Rozum, I., Schepers, D., Simmons, A., Soci, C., Dee, D. and Thepaut, J.-N. (2018a) ERA5 hourly data on pressure levels from 1959 to present. Copernicus Climate Change Service (C3S) Climate Data Store (CDS). https://doi.org/10.24381/cds.bd0915c6.

[Dataset] Hersbach, H., Bell, B., Berrisford, P., Biavati, G., Horanyi, A., Munoz Sabater, J., Nicolas, J., Peubey, C., Radu, R., Rozum, I., Schepers, D., Simmons, A., Soci, C., Dee, D. and Thepaut, J.-N. (2018b) ERA5 hourly data on single levels from 1959 to present. Copernicus Climate Change Service (C3S) Climate Data Store (CDS). https://doi.org/10.24381/cds.adbb2d47.

Hofsteenge, M. G., Cullen, N. J., Reijmer, C., van den Broeke, M., Katurji, M., Orwin, J. F. (2022) The surface energy balance during foehn events at Joyce Glacier, McMurdo Dry Valleys, Antarctica. The Cryosphere, 16, 5041-5059. https://doi.org/10.5194/tc-16-5041-2022.

Holland, P. R., Brisbourne, A., Corr, H. F. J., McGrath, D., Purdon, K., Paden, J., Fricker, H. A., Paolo, F. S. and Fleming, A. H. (2015) Oceanic and atmospheric forcing of Larsen C Ice-Shelf thinning. The Cryosphere, 9, 1005-1024. https://doi.org/10.5194/tc-9-1005-2015.

Holland, P. R., Feltham, D. L., Jenkins, A. (2007) Ice Shelf Water plume flow beneath Filchner-Ronne Ice Shelf, Antarctica. Journal of Geophysical Research, 112, C05044. https://doi.org/10.1029/2006JC003915.

[Dataset] Hunter, J. D. (2007) Matplotlib: A 2D graphics environment . Computing in Science and Engineering, 9, 90-95. https://doi.org/10.1109/MSCE.2007.55.

Hoskins, B. J. and Karoly, D. J. (1981) The Steady Linear Response of a Spherical Atmosphere to Thermal and Orographic Forcing. Journal of Atmospheric Sciences, 38(6), 1179-1996. https://doi.org/10.1175/1520-0469(1981)038<1179:TSLROA>2.0.CO;2.

~~Jacobs, S., Jenkins, A., Giulivi, C. and Dutrieux, P. (2011) Stronger ocean circulation and increased melting under Pine Island Glacier ice shelf. Nature Geosciences, 4, 519-523. https://doi.org/10.1038/ngeo1188.~~

Jenkins, A., Dutrieux, P., Jacobs, S. S., McPhail, S. D., Perrett, J. R., Webb, A. T. and White, D. (2010) Observations beneath Pine Island Glacier in West Antarctica and implications for its retreat. Nature Geosciences, 3, 468-472. https://doi.org/10.1038/ngeo890.

Joughin, I., Shapero, D., Smith, B., Dutrieux, P. and Barham, M. (2021) Ice-shelf retreat drives recent Pine Island Glacier speedup. Science Advances, 7(24). https://doi.org/10.1126/sciadv.abg3080.

Kaufman, Y. J., Tanre, D., Rmer, L. A., Vermote, E. F., Chu, A. and Holben, B. N. (1997) Operational remote sensing of tropospheric aerosol over land from EOS moderate resolution imaging spectroradiometer. Journal of Geophysical Research, 192, 17051-17067. https://doi.org/10.1029/96JD03988.

Kirchgaessner, A., King, J. C. and Anderson, P. S. (2021) The impact of Fohn conditions across the Antarctic Peninsula on local meteorology based on AWS measurements. Journal of Geophysical Research: Atmospheres, 126, e2020JD033748. https://doi.org/10.1029/2020JD033748.

Konrad, H., Hogg, A., Mulvaney, R., Arthern, R., Tuckwell, R., Medley, B., Shepherd, A. (2019) Observations of surface mass balance on Pine Island Glacier, West Antarctica, and the effect of strain history in fast-flowing sections. Journal of Glaciology, 65, 595-604. https://doi.org/10.1017/jog.2019.36.

Kowalewski, S., Helm, V., Morris, E. M. and Eisen, O. (2021) The regional-scale surface mass balance of Pine Island Glacier, West Antarctica, over the period 2005-2014, derived from airborne radar soundings and neutron probe measurements. The Crysophere, 15, 1285-1305. https://doi.org/10.5194/tc-15-1285-201.

Laffin, M. K., Zender, C. S., Singh, S., Van Wessem, J. M., Smeets, C. J. P. P. and Reijmer, C. H. (2021) Climatology and evolution of the Antarctic Peninsula fohn wind-induced melt regime from 1979-2018. Journal of Geophysical Research: Atmospheres, 126, e2020JD033682. https://doi.org/10.1029/2020JD033682.

[Dataset] Lazzara, M. (2022) Antarctic Meteorological Research Center & Automatic Weather Stations Project. Accessed on 06 November 2022, available online at http://amrc.ssec.wisc.edu/.

Lhermitte, S., Sun, S., Shuman, C., Wouters, B., Pattyn, F., Wuite, J., Berthier, E. and Nagler, T. (2021) Damage accelerates ice shelf instability and mass loss in Amundsen Sea Embayment. Proceeding of the National Academy of Sciences of the United States of America, 117(40), 24735-24741. https://doi.org/10.1073/pnas.1912890117.

Lestari, R. K. and Koh, T.-Y. (2016) Statistical Evidence for Asymmetry in ENSO-IOD Interactions. Atmosphere-Ocean, 54(5), 498-504. https://doi.org/10.1080/07055900.2016.1211084.

Li, S., Liao, J. and Zhang, L. (2022) Extraction and analysis of elevation changes in Antarctic ice sheet from CryoSat-2 and Sentinel-3 radar altimeters. Journal of Applied Remote Sensing, 16(3), 034514. https://doi.org/10.1117/1.JRS.16.034514.

Liu, S., Su, S., Cheng, Y., Tong, X. and Li, R. (2022) Long-Term Monitoring and Change Analysis of Pine Island Ice Shelf Based on Multi-Source Satellite Observations during 1973-2020. Journal of Marine Science and Engineering, 10, 976. https://doi.org/10.3390/jmse10070976.

Marshall, G. J. (2003) Trends in the Southern Annular Mode from observations and reanalyses. Journal of Climate, 16, 4134-4143. https://doi.org/10.1175/1520-0442%282003%29016<4134%3ATITSAM>2.0.CO%3B2.

Massom, R. A., Scambos, T. A., Bennetts, L. K., Reid, P., Squire, V. A. and Stammerjohn, S. E. (2018) Antarctic ice shelf disintegration triggered by sea ice loss and ocean swell. Nature, 558, 383-389. https://doi.org/10.1038/s41586-018-0212-1.

MacDonald, M. K., Pomeroy, J. W., Essery, R. L. H. (2018) Water and energy fluxes over northern prairies as affected by chinook winds and winter precipitation. Agricultural and Forest Meteorology, 248, 372-385. https://doi.org/10.1016/j.agrformet.2017.10.025.

Mclennan, M. L. and Lenaerts, J. T. M. (2021) Large-scale atmospheric drivers of snowfall over Thwaites Glacier, Antarctica. Geophysical Research Letters, 48, e2021GL093644. https://doi.org/10.1029/2021GL093644.

[Dataset] Met Office (2014) Cartopy: a cartographic python library with a Matplotlib interface. Accessed on 29 June 2022, available online at https://scitools.org.uk/cartopy.

~~Meredith, M. P., Inall, M. E., Brearley, J. A., Ehmen, T., Sheen, K., Munday, D., Cook, A., Retallick, K., Van Landeghem, K., Gerrish, L., Annett, A., Carvalho, F., Jones, R., Gabarato, A. C. N., Bull, C. S., Wallis, B. J., Hogg, A. E. and Scourse, J. (2022) Internal tsunamigenesis and ocean mixing driven by glacier calving in Antarctica. Science Advances, 8(47). https://doi.org/10.1126/sciadv.add0720.~~

Miles, B. W. J., Stokes, C. R. and Jamieson, S. S. R. (2017) Simultaneous disintegration of outlet glaciers in Porpoise Bay (Wilkes Land), East Antarctica, driven by sea ice break-up. The Cryosphere, 11, 427-442. https://doi.org/10.5194/tc-11-427-2017.

Moncada, J. M. and Holland, D. M. (2019) Automatic Weather Station Pine Island Glacier. United States Antarctic Program (USAP) Data Center. Accessed on 26 April 2022, https://doi.org/10.15784/601216.

Montesi, J., Elder, K., Schmidt, R. A., David, R. E. (2004) Sublimation of Intercepted Snow within a Subalpine Forest Canopy at Two Elevations. Journal of Hydrometeorology, 5, 763-773. https://doi.org/10.1175/1525-7541(2004)005<0763:SOISWA>2.0.CO;2.

Mottram, R., Hansen, N., Kittel, C., van Wessem, J. M., Agosta, C., Amory, C., Boberg, F., van de Berg, W., Fettweis, X., Gossart, A., van Lipzig, N. P. M., van Mejigaard, E., Orr, A., Phillips, T., Webster, S., Simonsen, S. B. and Souverijns, N. (2021) What is the surface mass balance of Antarctica? An intercomparison of regional climate model estimates. The Cryosphere, 15, 3751-3784. https://doi.org/10.5194/tc-15-3751-2021.

[Dataset] Mouginot, J., B. Scheuchl, and E. Rignot. 2017. MEaSUREs Antarctic Boundaries for IPY 2007-2009 from Satellite Radar, Version 2. Boulder, Colorado USA. NASA National Snow and Ice Data Center Distributed Active Archive Center. https://doi.org/10.5067/AXE4121732AD. Accessed on 8 November 2022.

Moussavi, M. S., Abdalati, W., Pope, A., Scambos, T., Tedesco, M., MacFerrin, M. and Grigsby, S. (2016) Derivation and validation of supraglacial lake volumes on the Greenland Ice Sheet from high-resolution satellite imagery. Remote Sensing of Environment, 183, 294-303. https://doi.org/10.1016/j.rse.2016.05.024.

[Dataset] NASA (National Aeronautics and Space Administration) / LARC (Langley Research Center) / SD (Science Division) / ASDC (Atmospheric Data Center) (2017) CERES and GEO-Enhanced TOA, Within-Atmosphere and Surface Fluxes, Clouds and Aerosols 1-Hourly Terra-Aqua Edition4A. NASA Langley Atmospheric Science Data Center DAAC. Retrieved from https://doi.org/10.5067/TERRA+AQUA/CERES/SYN1DEG-1HOUR_L3.004A.

Nilsson, J., Gardner, A. S. and Paolo, F. S. (2022) Elevation change of the Antarctic Ice Sheet: 1985 to 2020. Earth System Science Data, 14, 3573-3598. https://doi.org/10.5194/essd-14-3573-2022.

Orr, A., Deb, P., Clem, K. R., Gilbert, E., Bromwich, D. H., Boberg, F., Colwell, S., Hansen, N., Lazzara, M. A., Mooney, P. A., Mottram, R., Niwano, M., Phillips, T., Pishniak, D., Reijmer, C. H., van de Berg, W. J., Webster, S. and Zuo, X. (2022) Characteristics of surface “melt potential” over Antarctic ice shelves

based on regional atmospheric model simulations of summer air temperature extremes from 1979/80 to 2018/19. Journal of Climate, 1-61. https://doi.org/10.1175/JCLI-D-22-0386.1.

Pohl, B., Fauchereau, N., Reason, C. J. C. and Rouault, M. (2010) Relationships between the Antarctic Oscillation, the Madden-Julian Oscillation, and ENSO, and Consequences for Rainfall Analysis. Journal of Climate, 23(2), 238-254. https://doi.org/10.1175/2009JCLI2443.1.

Polvani, L. M., Banerjee, A., Chemke, R., Doddridge, E. W., Ferreira, D., Gnanadesikan, A., Holland, M. A., Kostov, Y., Marshall, J., Seviour, W. J. M., Solomon, S. and Waugh, D. W. (2021) Interannual SAM modulation of Antarctic sea ice extent does not account for its long-term trends, pointing to a limited role for ozone depletion. Geophysical Research Letters, 48, e2021GL098471. https://doi.org/10.1029/2021GL094871.

Ponti, S., Scipionotti, R., Pierattini, S., Guglielmin, M. (2021) The Spatio-Temporal Variability of Frost Blisters in a Perennial Frozen Lake along the Antarctic Coast as Indicator of the Goundwater Supply. Remote Sensing, 13, 435. https://doi.org/10.3390/rs13030435.

Pradhananga, D., Pomeroy, J. W. (2022) Diagnosing changes in glacier hydrology from physical principles using a hydrological model with snow redistribution, sublimation, firnification and energy balance ablation algorithms. Journal of Hydrology, 608, 127545. https://doi.org/10.1016/j.jhydrol.2022.127545.

Quintanar, A. I. and Mechoso, C. R. (1995a) Quasi-Stationary Waves in the Southern Hemisphere. Part I: Observational Data. Journal of Climate, 8(11), 2659-2672. https://doi.org/10.1175/1520-0442(1995)008<2659:QSWITS>2.0.CO;2.

Quintanar, A. I. and Mechoso, C. R. (1995b) Quasi-Stationary Waves in the Southern Hemisphere. Part II: Generation Mechanisms. Journal of Climate, 8(11), 2673-2690. https://doi.org/10.1175/1520-0442(1995)008<2673.QSWITS>2.0.CO;2.

Raphael, M. N., Marshall, G. J., Turner, J., Fogt, R. L., Schneider, D., Dixon, D. A., Hosking, J. S., Jones, J. M. and Hobbs, W. R. (2016) The Amundsen Sea Low: Variability, Change, and Impact on Antarctic Climate. Bulletin of the American Meteorological Society, 97(1), 111-121. https://doi.org/10.1175/BAMS-D-14-00018.1.

Reijmer, C., Greuell, W. and Oerlemans, J. (1999) The annual cycle of meteorological variables and the surface energy balance on Berkner Island, Antarctica. Annals of Glaciology, 29, 49-54. https://doi.org/10.3189/172756499781821166.

[Dataset] Rignot, E., Mouginot, J. and Scheuchl, B. (2017) MEaSUREs InSAR-Based Antarctica Ice Velocity Map, Version 2. Boulder, Colorado USA. National Aeronautics and Space Administration National Snow and Ice Data Center Distributed Active Archive Center. Accessed on 26 April 2022, available online at https://doi.org/10.5067/D7GK8F5J8M8R.

Rintoul, S. R., Silvano, A., Pena-Molino, B., Wijk, E. V., Rosenberg, M., Geenbaum, J. E., Blankenship, D. (2016) Ocean heat drives rapid basal melt of the Totten Ice Shelf. Science Advances, 2. https://doi.org/10.1126/sciadv.1601610.

Rogers, R. R., Yau, M. K. (1989) A Short Course in Cloud Physics, 3rd edition. Pergamon, New York, 293 pp.

Rosier, S. H. R., Reese, R., Donges, J. F., De Rydt, J., Gudmundsson, G. H. and Winkelmann, R. (2021) The tipping points and early warning indicators for Pine Island Glacier, West Antarctica. The Cryosphere, 15, 1501-1516. https://doi.org/10.5194/tc-15-1501-2021.

Rousseeux, P. J. (1987) Silhouettes: A graphical aid to the interpretation and validation of cluster analysis. Journal of Computational and Applied Mathematics, 20, 53-65. https://doi.org/10.1016/0377-0427(87)90125-7.

Scarchilli, C., Frezzotti, M., Grigioni, P., De Silvestri, L., Agnoletto, L., Dolci, S. (2010) Extraordinary blowing snow transport events in East Antarctica. Climate Dynamics, 34, 1195-1206. https://doi.org/10.1007/s00382-009-0601-0.

Scott, R. C., Nicolas, J. P., Bromwich, D. H., Norris, J. R. and Lubin, D. (2019) Meteorological Drivers and Large-Scale Climate Forcing of West Antarctic Surface Melt. Journal of Climate, 32(3), 665-684. https://doi.org/10.1175/JCLI-D-18-0233.1.

Silber, I., Verlinde, J., Wang, S.-H., Bromwich, D. H., Fridlind, A. M., Cadeddu, M., Eloranta, E. W. and Flynn, C. J. (2019) Cloud Influence on ERA5 and AMPS Surface Downwelling Longwave Radiation Biases in West Antarctica. Journal of Climate, 32(22), 7935-7949. https://doi.org/10.1175/JCLI-D-19-0149.1.

Simmonds, I., Keay, K. and Lim, E.-P. (2003) Synoptic Activity in the Seas around Antarctica. Monthly Weather Review, 131(2), 272-288. https://doi.org/10.1175/1520-0493(2003)131<0272:SAITSA>2.0.CO;2

Smith, B., Fricker, H. A., Gardner, A. S., Medley, B., Nilsson, J., Paolo, F. S., Holschuh, N., Adusumilli, S., Brunt, K., Csatho, B., Harbeck, K., Markus, T., Neumann, T., Siegfried, M. R. and Zwally, H. J. (2020) Pervasive ice sheet mass loss reflects competing ocean and atmosphere processes. Science, 368, 1239-1242. https://doi.org/10.1126/science.aaz5845.

Speirs, J. C., McGowan, H. A., Steinhoff, D. F. and Bromwich, D. H. (2013) Regional climate variability driven by foehn winds in the McMurdo Dry Valleys, Antarctica. International Journal of Climatology, 33, 945-958. https://doi.org/10.1002/joc.3481.

~~Speirs, J. C., Steinhoff, D. F., McGowan, H. A., Bromwich, D. H. and Monaghan, A. J. (2010) Foehn Winds in the McMurdo Dry Valleys, Antarctica: The Origin of Extreme Warming Events. Journal of Climate, 23(13), 3577-3598. https://doi.org/10.1175/2010JCLI3382.1.~~

Stanton, T. P., Shaw, W. J., Truffer, M., Corr, H. F. J., Peters, L. E., Riverman, K. L., Bindschadler, R., Holland, D. M. and Anandakrishnan, S. (2013) Channelized Ice Melting in the Ocean Boundary Layer Beneath Pine Island Glacier, Antarctica. Science, 341, 1236-1239. https://doi.org/10.1126/science.1239373.

Steinley, D. (2006) K-means clustering: A half-century synthesis. British Journal of Mathematical and Statistical Psychology, 59, 1-34. https://doi.org/10.1348/000711005X48266.

Stigter, E. E., Litt, M., Steiner, J. F., Bonekamp, P. N. J., Shea, J. M., Bierkens, M. F. P. and Immerzeel, W. W. (2018) The Importance of Snow Sublimation on a Himalayan Glacier. Frontiers in Earth Sciences, 6, 108. https://doi.org/10.3389/feart.2018.00108.

The IMBIE team (2018) Mass balance of the Antarctic Ice Sheet from 1992 to 2017. Nature, 558, 219-222. https://doi.org/10.1038/s41586-018-0179-y.

Tian, L., Li, H., Li, F., Li, X., Du, X. and Ye, X. (2018) Identification of key influence factors and an empirical formula for spring snowmelt-runoff: A case study in mid-temperate zone of northeast China. Scientific Reports, 8, 16950. https://doi.org/10.1038/s41598-018-35282-x.

~~Toyota, T., Massom, R., Tateyama, K., Tamura, T., Fraser, A. (2011) Properties of snow overlying the sea ice off East Antarctica in late winter, 2007. Deep Sea Research Part II: Topical Studies in Oceanography, 58, 1137-1148. https://doi.org/10.1016/j.dsr2.2010.12.002.~~

Turner, J. (2004) The El Nino-Southern Oscillation and Antarctica. International Journal of Climatology, 24, 1-31. https://doi.org/10.1002/joc.965.

Turner, J., Phillips, T., Hosking, J. S., Marshall, G. J. and Orr, A. (2013) The Amundsen Sea low. International Journal of Climatology, 33, 1818-1829. https://doi.org/10.1002/joc.3558.

van den Broeke, M. R. (1997) Spatial and temporal variation of sublimation on Antarctica: Results of a high-resolution general circulation model. Journal of Geophysical Research, 102, 29765-29777. https://doi.org/10.1029/97JD01862.

[Dataset] Vermote, E. (2015a) MOD09CMG MODIS Surface Reflectance Daily L3 Global 0.05Deg CMG. NASA EOSDIS Land Processes DAAC. http://doi.org/10.5067/MODIS/mod09cmg.006.

[Dataset] Vermote, E. (2015b) MYD09CMG MODIS Surface Reflectance Daily L3 Global 0.05Deg CMG. NASA EOSDIS Land Processes DAAC. http://doi.org/10.5067/MODIS/myd09cmg.006.

Webber, B. G. M., Heywood, K. J., Stevens, D. P., Dutrieux, P., Abrahamsen, E. P., Jenkins, A., Jacobs, S. S. , Ha, H. K., Lee, S. H. and Kim, T. W. (2017) Mechanisms driving variability in the ocean forcing of Pine Island Glacier. Nature Communications, 8, 14507. https://doi.org/10.1038/ncomms14507.

Wiesenekker, J. M., Munneke, P. K., Van den Broeke, M. R. and Smeets, C. J. P. P. (2018) A Multidecadal Analysis of Fohn Winds over Larsen C Ice Shelf from a Combination of Observations and Modeling. Atmosphere, 9(5), 172. https://doi.org/10.3390/atmos9050172.

~~Willie, J. D., Favier, V., Dufour, A., Gorodetskaya, I. V., Turner, J., Agosta, C. and Codron, F. (2019) West Antarctic surface melt triggered by atmospheric rivers. Nature Geosciences, 12, 911-916. https://doi.org/10.1038/s41561-019-0460-1.~~

Willie, J. D., Favier, V., Gorodetskaya, I. V., Agosta, C., Kittel, C., Beeman, J. C., Jourdain, N. C., Lenaerts, J. T. M. and Codron, F. (2021) Antarctic atmospheric river climatology and precipitation impacts. Journal of Geophysical Research: Atmospheres, 126, e2020JD033788. https://doi.org/10.1029/2020JD033788.

~~Willie, J. D., Favier, V., Jourdain, N. C., Kittel, C., Turton, J. V., Agosta, C., Gorodetskaya, I. V., Picard, G., Codron, Santos, C. L. D., Amory, C., Fettweis, X., Blanchet, J., Jomelli, V. and Berchet, A. (2022) Intense atmospheric rivers can weaken ice shelf stability at the Antarctic Peninsula. Communications Earth & Environment, 3, 90. https://doi.org/10.1038/s43247-022-00422-9.~~

Wingham, D. J., Wallis, D. W. and Shepherd, A. (2009) Spatial and temporal evolution of Pine Island Glacier thinning, 1995-2006. Geophysical Research Letters, 36, L17501. https://doi.org/10.1029/2009GL039126.

~~Yang, J., Yau, M. K., Fang, X., Pomeroy, J. W. (2010) A triple-moment blowing snow-atmospheric model and its application in computing the seasonal wintertime snow mass budget. Hydrology and Earth System Sciences, 14, 1063-1079. https://doi.org/10.5194/hess-14-1063-2010.~~

Yuan, X. (2004) ENSO-related impacts on Antarctic sea ice: a synthesis of phenomenon and mechanisms. Antarctic Science, 16(4), 415-425. https://doi.org/10.1017/S0954102004002238.

Yuan, X. and Martinson, D. G. (2001) The Antarctic dipole and its predictability. Geophysical Research Letters, 28, 3609-3612. https://doi.org/10.1029/2001GL012969.

Zhang, X., Wu, B. and Ding, S. (2022) Combined effects of La Nina events and Arctic tropospheric warming on the winter North Pacific storm track. Climate Dynamics. https://doi.org/10.1007/s00382-022-06389-9.

Zheng, M. and Li, X., (2022) Distinct patterns of monthly Southern Annular Mode events. Atmospheric and Oceanic Science Letters, 15, 100206. https://doi.org/10.1016/j.aosl.2022.100206.

Zou, X., Bromwich, D. H., Montenegro, A., Wang, S.-H. and Bai, L. (2021a) Major surface melting over the Ross Ice Shelf part I: Foehn effect. Quarterly Journal of the Royal Meteorological Society, 147, 2874-2894. https://doi.org/10.1002/qj.4104.

Zou, X., Bromwich, D. H., Montenegro, A., Wang, S.-H. and Bai, L. (2021b) Major surface melting over the Ross Ice Shelf part II: Surface energy balance. Quarterly Journal of the Royal Meteorological Society, 147, 2895-2916. https://doi.org/10.1002/qj.4105.

Zou, X., Bromwich, D. H., Nicholas, J. P., Montenegro, A. and Wang, S.-H. (2019) West Antarctic surface melt event of January 2016 facilitated by fohn warming. Quarterly Journal of the Royal Meteorological Society, 145, 687-784. https://doi.org/10.1002/qj.3460.